JOURNAL OF PETROLOGY | VOLUME 48 | NUMBER 8 | PAGES 1443–1470 | 2007 | doi:10.1093/petrology/egm024

Petrology and Geochronology of Granulites from the McKaskle Hills, Eastern Amery Ice Shelf, Antarctica, and Implications for the Evolution of the Prydz Belt

XIAOCHUN LIU[1]*, YUE ZHAO[1], GUOCHUN ZHAO[2], PING JIAN[3] AND GANG XU[1]

[1]INSTITUTE OF GEOMECHANICS, CHINESE ACADEMY OF GEOLOGICAL SCIENCES, BEIJING 100081, CHINA
[2]DEPARTMENT OF EARTH SCIENCES, THE UNIVERSITY OF HONG KONG, POKFULAM ROAD, HONG KONG, CHINA
[3]SHRIMP LABORATORY, INSTITUTE OF GEOLOGY, CHINESE ACADEMY OF GEOLOGICAL SCIENCES, BEIJING 100026, CHINA

RECEIVED FEBRUARY 10, 2006; ACCEPTED APRIL 4, 2007
ADVANCE ACCESS PUBLICATION JUNE 7, 2007

A combined petrological and geochronological study was carried out on mafic granulites and associated felsic gneisses from the McKaskle Hills, eastern Amery Ice Shelf, East Antarctica. Garnet-bearing mafic granulites exhibit reaction textures and exsolution textures that indicate two-stage metamorphic evolution. Thermobarometric estimates from matrix and symplectite assemblages yield peak and retrograde P–T *conditions of 9·0–9·5 kbar and 880–950°C and 6·6–7·2 kbar and 700–750°C, respectively. Similar but slightly scattered peak* P–T *estimates of 7·9–10·1 kbar and 820–980°C are obtained from the core compositions of minerals from felsic para- and orthogneisses. Evidence for the prograde history is provided by muscovite inclusions in garnet from a paragneiss. Sensitive high-resolution ion microprobe U–Pb zircon dating reveals an evolutionary history for the granulites, including a mafic and felsic igneous intrusion at 1174–1019 Ma, sedimentation after 932–916 Ma, and a high-grade metamorphism at 533–529 Ma. In contrast, Sm–Nd mineral–whole-rock dating mainly yields a single age population at ~500 Ma. This suggests that the McKaskle Hills form part of the Prydz Belt, and that the relatively high peak* P–T *conditions and a decompression-dominated* P–T *path for the rocks resulted from a single Cambrian metamorphic cycle, rather than two distinct metamorphic events as formerly inferred for the granulites from Prydz Bay. The age data also indicate that the Precambrian history of the McKaskle Hills is not only distinct from that of the early Neoproterozoic terrane in the northern Prince Charles Mountains, but also different from that of other parts of the Prydz Belt. The existence of multiple basement terranes, together with considerable crustal thickening followed by tectonic uplift and unroofing indicated by the clockwise* P–T–t *evolution, suggests that the Prydz Belt may represent a collisional orogen that resulted in the assembly of Gondwana during the Cambrian period.*

KEY WORDS: *Mesoproterozoic basement; Cambrian metamorphism; P–T path; Prydz Belt; East Antarctica*

INTRODUCTION

One of the most important developments made in the field of Antarctic geology over the last decade is the recognition and confirmation of late Neoproterozoic–Cambrian (also termed Pan-African) high-grade tectonothermal events in East Antarctica. This has led to the breakdown of the concept of a single continuous late Mesoproterozoic–early Neoproterozoic (i.e. Grenvillian) Circum-East Antarctic Mobile Belt and, therefore, has challenged traditional Rodinia reconstructions (Dalziel, 1991; Hoffman, 1991; Moores, 1991). Between two major early Neoproterozoic–Cambrian orogenic belt systems in East Antarctica, most geologists have considered the Lützow–Holm Belt and

*Corresponding author. Telphone: +86-10-68486756. Fax: +86-10-68422326. E-mail: liuxchqw@yahoo.com.cn

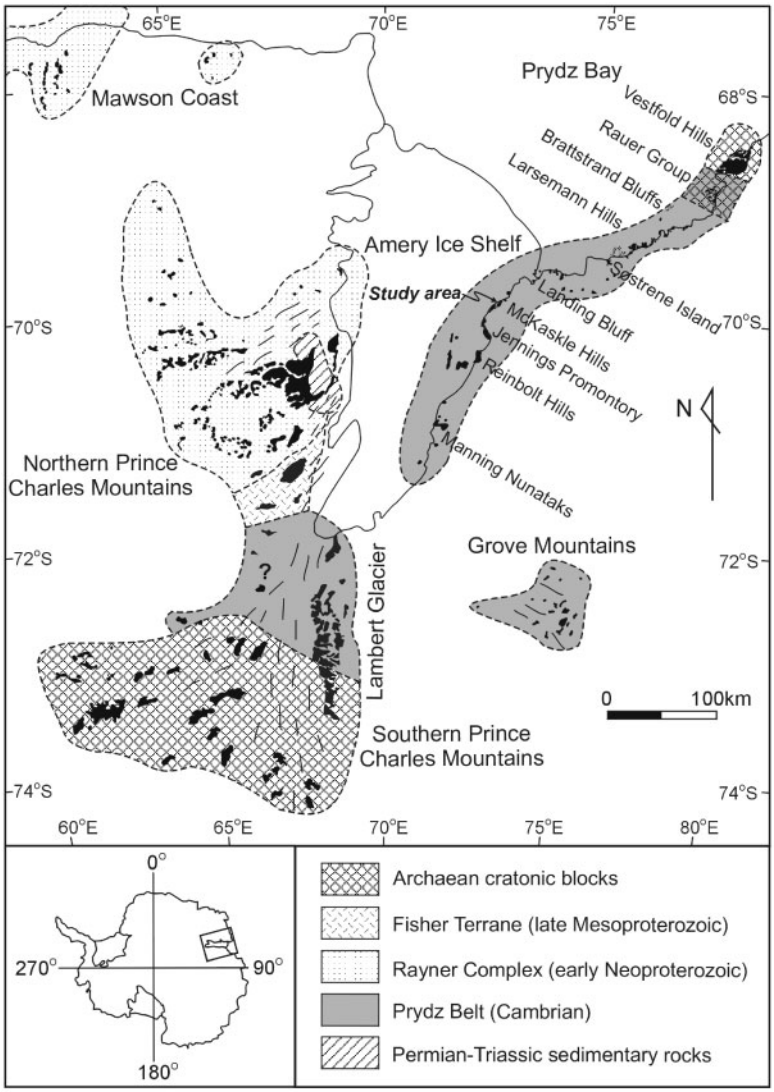

Fig. 1. Geological sketch map of the Prince Charles Mountains–Prydz Bay area and its location in East Antarctica (modified after Mikhalsky *et al.*, 2001; Fitzsimons, 2003).

central Dronning Maud Land as a southern continuation of the East African Orogen, which could have resulted from the final collision between East and West Gondwana (e.g. Shiraishi *et al.*, 1994; Shackleton, 1996; Jacobs *et al.*, 1998, 2003; Fitzsimons, 2000). However, the Prydz Belt and Denman Glacier are located in the interior of what was previously considered to be a unified East Gondwana block and preserve polyphase tectonothermal histories of Archaean to early Palaeozoic age. Hence the nature and role of Cambrian tectonism in these areas in the assembly of Gondwana remain a subject for debate (Fitzsimons, 2003; Harley, 2003; Yoshida *et al.*, 2003; Zhao *et al.*, 2003, and references therein).

The eastern Amery Ice Shelf (EAIS) lies near the boundary between the Cambrian high-grade complex of Prydz Bay and the early Neoproterozoic high-grade complex of the northern Prince Charles Mountains (nPCM) (Fig. 1), and could be a key area for understanding the tectonic evolution of the Prydz Belt. Earlier studies suggested that rocks exposed in the Reinbolt Hills were metamorphosed under low- to medium-pressure granulite-facies conditions and were assumed to be related to an early Neoproterozoic tectonothermal event based on the occurrence of a synmetamorphic pegmatite with a U–Pb zircon age of 896 Ma (Grew & Manton, 1981; Nichols & Berry, 1991). However, a Th–U–total Pb monazite age of 536 Ma recently obtained from a sillimanite-bearing pegmatite has led to a suggestion that the area may have been affected by a Cambrian metamorphic event (Ziemann *et al.*, 2005). As no geochronological constraints are available for the metamorphic rocks, it is difficult to determine the timing of regional high-grade

metamorphism in the EAIS and to determine whether or not the area has experienced poly-phase metamorphism as inferred from Prydz Bay (Henson & Zhou, 1995; Hensen *et al.*, 1995).

To investigate the above issues, we undertook a petrological and geochronological study of garnet-bearing mafic granulites and associated felsic gneisses exposed in the McKaskle Hills, northern EAIS. We deduce a clockwise P–T path for these rocks based on mineral reaction textures and thermobarometric calculations and demonstrate that this P–T path is related to a single Cambrian metamorphic event on the basis of sensitive high-resolution ion microprobe (SHRIMP) U–Pb zircon dating and Sm–Nd mineral-whole-rock dating. These new data are then used to discuss the tectonic setting of the EAIS and the evolution of the Prydz Belt in the context of Gondwana assembly.

REGIONAL FRAMEWORK AND FIELD RELATIONS

The Prince Charles Mountains–Prydz Bay area comprises low- to high-grade metamorphic rocks only within distinct crustal blocks that range in age from Archaean to late Mesoproterozoic–early Neoproterozoic and Cambrian (Fig. 1). Three Archaean blocks, exposed in the Vestfold Hills, Rauer Group and southern Prince Charles Mountains (sPCM), preserve distinct crustal histories and therefore do not form remnants of a single unified craton (Harley, 2003). The Vestfold Hills are dominated by granulite-facies orthogneiss interlayered with metapelitic supracrustal rocks. Metamorphism, deformation and subsequent mafic–felsic intrusion were dated between 2520 Ma and 2480 Ma (Black *et al.*, 1991; Snape *et al.*, 1997). The Rauer Group is a composite terrane containing Archaean (>3300 Ma and ~2840–2800 Ma) tonalitic orthogneisses and late Mesoproterozoic (1030–1000 Ma) mafic to felsic intrusive rocks (Kinny *et al.*, 1993; Harley *et al.*, 1998). Both rock types have been recrystallized during Cambrian high-grade metamorphism (Harley *et al.*, 1998; Kelsey *et al.*, 2003*a*). The sPCM comprises Archaean (~3200–3000 Ma) granitic gneiss basement interleaved with sedimentary rocks of different age groups (Tingey, 1991; Mikhalsky *et al.*, 2001; Boger *et al.*, 2006; Phillips *et al.*, 2006). This basement and at least some of the sedimentary rocks underwent greenschist- to amphibolite-facies metamorphism and deformation prior to 2650 Ma (Boger *et al.*, 2001, 2006).

Late Mesoproterozoic rocks are exposed in the southern sector of the nPCM (i.e. Fisher terrane), where mafic–felsic volcanism and intrusion occurred at 1300–1020 Ma, followed by amphibolite-facies metamorphism at 1020–940 Ma (Beliatsky *et al.*, 1994; Kinny *et al.*, 1997; Mikhalsky *et al.*, 1999). Nd model ages (T_{DM}) for these igneous rocks range from 1780 to 1360 Ma (Mikhalsky *et al.*, 2006). Early Neoproterozoic rocks in the nPCM and adjacent Mawson Coast (i.e. Rayner Complex) are characterized by granulite-facies metamorphism accompanied by widespread charnockitic and granitic magmatism dated at 990–900 Ma (Manton *et al.*, 1992; Kinny *et al.*, 1997; Boger *et al.*, 2000; Carson *et al.*, 2000). The T_{DM} ages of the granitoids range from 2160 to 1600 Ma (Young *et al.*, 1997; Zhao *et al.*, 1997*a*). Metamorphism is of high-temperature, low- to medium-pressure type (6–8 kbar and 800–880°C), characterized by an isobaric cooling P–T path (Fitzsimons & Harley, 1992, 1994a; Hand *et al.*, 1994; Stephenson & Cook, 1997; Boger & White, 2003). In addition, intraplate deformation and emplacement of minor pegmatite sheets at 550–500 Ma have been observed in some places (Carson *et al.*, 2000; Boger *et al.*, 2002). This may be a response to the intense Cambrian tectonism that occurred in the Prydz Belt.

The Prydz Belt mainly crops out along the Prydz Bay coast (Fig. 1). Equivalently or similarly aged rocks are also exposed in the Grove Mountains (Zhao *et al.*, 2000; Liu *et al.*, 2002) and in the northern part of the sPCM (Boger *et al.*, 2001; Corvino *et al.*, 2005). The high-grade metamorphic rocks in Prydz Bay comprise two lithological associations: mafic–felsic composite orthogneisses and migmatitic paragneisses, which are attributed to the basement and cover sequences, respectively (Fitzsimons & Harley, 1991; Dirks & Hand, 1995; Dirks & Wilson, 1995). Geochronological studies suggest that the basement orthogneisses were formed at ~1100 Ma with T_{DM} ages of 2300–1800 Ma (Hensen & Zhou, 1995; Zhao *et al.*, 1995, 2003; Wang *et al.*, 2003), whereas the cover sequence is assumed to have been deposited during the late Mesoproterozoic (Dirks & Wilson, 1995; Carson *et al.*, 1996) or Neoproterozoic (Hensen & Zhou, 1995; Zhao *et al.*, 1995). The peak metamorphic P–T conditions in different localities of the area have been estimated at 6–7 kbar and 760–860°C, followed by a P–T path involving near-isothermal decompression (Motoyoshi *et al.*, 1991; Fitzsimons, 1996; Carson *et al.*, 1997). The major tectonothermal events, including deformation, high-grade metamorphism and emplacement of syn- to post-orogenic granites, took place between 550 Ma and 490 Ma (Zhao *et al.*, 1992, 1997b, 2000; Hensen & Zhou, 1995; Carson *et al.*, 1996; Zhang *et al.*, 1996; Fitzsimons *et al.*, 1997). In addition, an earlier, relatively high-pressure event (9–10 kbar and 850–980°C) is preserved in some areas (Thost *et al.*, 1991; Ren *et al.*, 1992; Tong & Liu, 1997). In rocks from Søstrene Island, this event has been dated at ~990 Ma using the Sm–Nd isochron method (Hensen *et al.*, 1995). The rocks from the Grove Mountains record peak P–T conditions (6·1–6·7 kbar and 850°C) similar to those from Prydz Bay (Liu *et al.*, 2003). However, in the rocks of the sPCM, Cambrian peak metamorphic

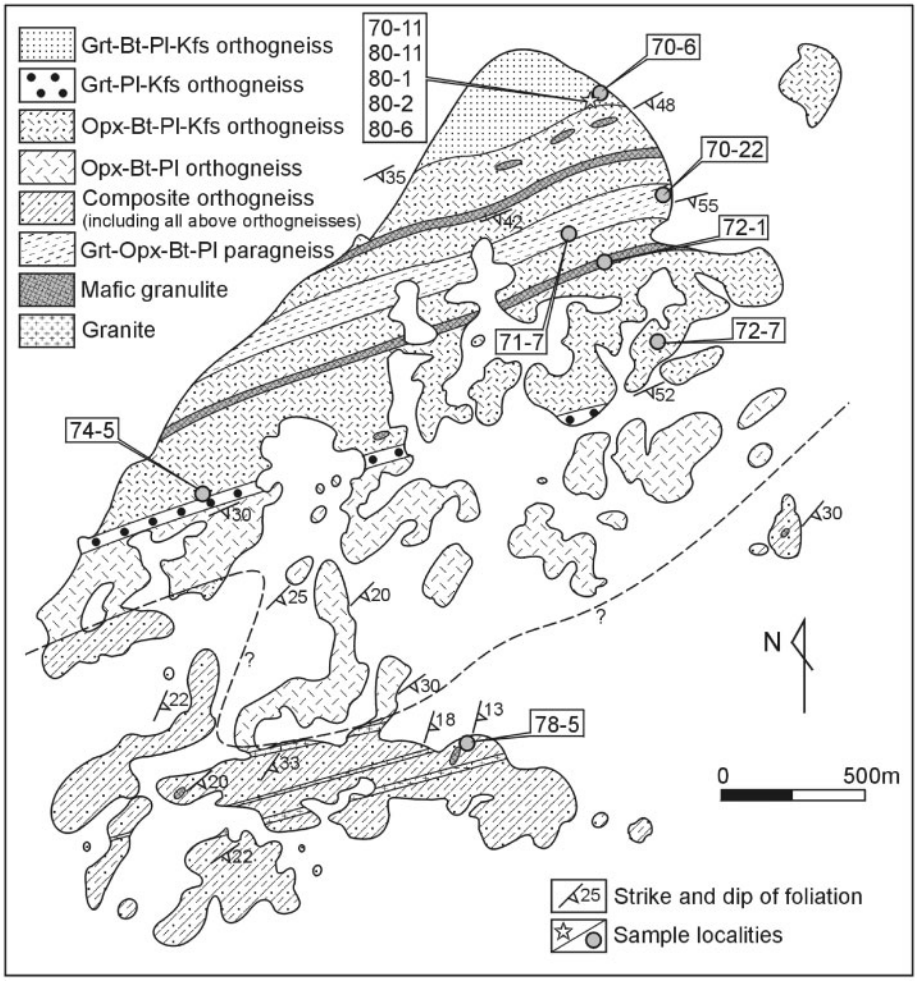

Fig. 2. Geological map of the McKaskle Hills showing sampling localities. Mineral abbreviations are after Kretz (1983).

temperatures reach only 650–700°C at 6–7 kbar (Boger & Wilson, 2005).

The principal outcrops in the EAIS area (Manning Nunataks, Reinbolt Hills, Jennings Promontory, McKaskle Hills and Landing Bluff) are dominated by orthopyroxene-bearing orthogneisses interleaved with minor paragneisses, calc-silicate rocks and mafic granulites (Tingey, 1981; Sheraton *et al.*, 1996). Although a few Neoproterozoic–Cambrian ages have been reported for some pegmatites in the Reinbolt Hills (Grew & Manton, 1981; Ziemann *et al.*, 2005) and from granites in Landing Bluff (Tingey, 1991), the timing of regional high-grade metamorphism remains poorly constrained. The McKaskle Hills in the northern EAIS mainly consist of brown, layered or massive orthopyroxene-bearing orthogneisses. These rocks contain variable amounts of biotite, plagioclase, K-feldspar and Fe–Ti oxides (Fig. 2). Garnet, clinopyroxene and amphibole may additionally be present but all three of these minerals never coexist in one sample. Pale garnet-bearing but orthopyroxene-absent orthogneiss and garnet–orthopyroxene-bearing paragneiss are also present in the northern McKaskle Hills. Thin calc-silicate bands comprising garnet, clinopyroxene, scapolite and plagioclase are interleaved with the paragneiss. The original relationships between these metasedimentary rocks and the orthogneisses have been obliterated by deformation and metamorphism. Two-pyroxene mafic granulites are widespread. These rocks mostly occur as irregular blocks, lenses or layers (1–15 m wide) in various orthogneisses. Many layers of mafic granulite define open–tight folds and preserve axial-planar foliation that is parallel to the gneissosity of the host gneisses. Garnet-bearing mafic granulite occurs in garnet-bearing orthogneiss at the northeastern end of the outcrops (70°00′24″S, 72°59′29″E). This unit is relatively small, forming a 1·5 m wide layer that extends more than 10 m along the strike (Fig. 3). In addition, a number of shallowly dipping (10–15°) granitic dykes with widths of several metres occur in the southern McKaskle Hills. These dykes obliquely cut the foliation of country gneisses and are assumed to be Cambrian intrusions.

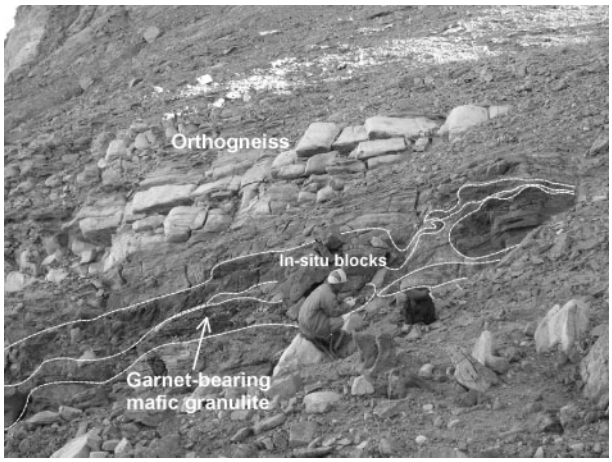

Fig. 3. Photograph showing the field relationship of a garnet-bearing mafic granulite from the McKaskle Hills.

SAMPLES AND ANALYTICAL TECHNIQUES

Eleven garnet- and orthopyroxene-bearing samples were selected for detailed petrological study. These samples include five mafic granulites (70-11, 80-11, 80-1, 80-2 and 80-6), three felsic paragneisses (70-6, 70-22 and 71-7), and three felsic orthogneisses (72-7, 74-5 and 78-5, Fig. 2). A garnet-bearing mafic granulite (sample 80-1), a garnet-free mafic granulite (sample 72-1), a paragneiss (sample 71-7) and an orthogneiss (sample 72-7) were chosen for SHRIMP U–Pb zircon dating. Two garnet-bearing mafic granulites (samples 70-11 and 80-1) and two paragneisses (samples 70-6 and 71-7) were chosen for Sm–Nd mineral–whole-rock dating. These samples are all fresh and most appear to have avoided partial melting, except for some paragneisses.

The chemical compositions of the constituent minerals were analyzed using a JEOL JXA-8100 wavelength-dispersive electron microprobe at the MOE Key Laboratory of Orogenic Belts and Crustal Evolution of Peking University. The operating conditions were 15 kV accelerating voltage, a 10 nA beam current and a counting time of 10 s for each peak. The beam diameter was set to 2 μm for all minerals except for orthopyroxene lamellae (1 μm) and for micas (5 μm). Natural minerals were used as standards. Ferric iron in garnet, clinopyroxene and orthopyroxene was calculated based on the scheme of Droop (1987). Molecular formulae for amphibole were calculated based on Holland & Blundy (1994), with modifications following Dale *et al.* (2000). Ferric iron in biotite was estimated based on the assumption of $Fe^{3+}/(Fe^{2+}+Fe^{3+}) = 0.116$ (Holdaway *et al.*, 1997). Total iron is reported as ferrous iron in muscovite. Representative mineral analyses are presented in Table 1. Mineral abbreviations are after Kretz (1983), except for amphibole (Amp).

In an attempt to determine reintegrated pyroxene compositions (i.e. lamellae + host), we employed point reintegrations via spot analyses using a defocused beam (see Liu *et al.*, 2003). Specifically, the microprobe beam was defocused to 25 μm width, and 20 spots were collected equidistantly across grains containing regularly spaced lamellae. The spot analyses were then averaged to provide a reintegrated composition for each pyroxene.

Zircon analyses were performed using the SHRIMP II ion microprobe at the Beijing SHRIMP Centre, Chinese Academy of Geological Sciences. Zircons were extracted from the samples using conventional techniques, including crushing, sieving, heavy liquid separation and hand-picking. Zircon grains were mounted in an epoxy disc along with the TEMORA zircon standard and polished down to expose their centres. The internal structures of the zircons were characterized by cathodoluminescence (CL) imaging. Instrumental conditions and data acquisition procedures are the same as described by Williams (1998). A primary ion beam of 4·5 nA, 10 kV O_2^- and ~20 μm spot were used. The data were collected in sets of five scans per dataset with analyses of the unknown zircons interspaced with analyses of the reference zircon every three analyses. The measured $^{206}Pb/^{238}U$ ratios were corrected using reference zircon TEMORA (416·75 ± 0·24 Ma; Black *et al.*, 2003). Correction for common Pb was made using the measured ^{204}Pb and assuming a model common Pb composition (Stacey & Kramers, 1975) appropriate to the age of the mineral. The age uncertainties for individual analyses represent 1σ, but the weighted mean $^{206}Pb/^{238}U$ or $^{207}Pb/^{206}Pb$ ages calculated using the computer program Isoplot (version 2.06; Ludwig, 1999) are quoted at the 95% confidence level.

Mineral–whole-rock Sm–Nd isotopic analyses were conducted at the Institute of Geology and Geophysics, Chinese Academy of Sciences. Garnet, clinopyroxene, orthopyroxene, biotite and plagioclase were separated using a magnetic separator followed by hand-picking under a binocular microscope. The analytical procedures are the same as those reported by Yang *et al.* (2004). Powder samples were weighed and spiked with ^{149}Sm and ^{150}Nd and then dissolved in acid ($HF + HNO_3$). Dissolution was carried out in Teflon vials at about 100°C for 12 days. Sm and Nd were separated using conventional ion exchange procedures. Mass analysis was performed using a VG 354 multicollector mass spectrometer. Nd isotopic fractionation was corrected assuming $^{146}Nd/^{144}Nd = 0·7219$. During the period of data acquisition, the measured isotope ratios for the La Jolla Nd standard was $^{143}Nd/^{144}Nd = 0·511862 \pm 0·000007$ (2σ, $n = 6$). Total procedural blanks were <100 pg. Sm–Nd isochron ages were also calculated using the Isoplot program of Ludwig (1999). Input errors (2σ) used in age calculations are $^{147}Sm/^{144}Nd = 1\%$ and $^{143}Nd/^{144}Nd = 0·005\%$.

Table 1: Representative microprobe analyses of minerals from mafic granulites and felsic gneisses

	80-11 (mafic granulite)																	
Mineral:	Grt	Grt	Cpx	Cpx	Cpx	Cpx	Cpx	Opx	Opx	Opx	Opx	Opx	Amp	Amp	Amp	Bt	Pl	Pl
Domain:	core	rim	incl.	reint.	core	rim	sympl.	incl.	reint.	core	lam.	sympl.	incl.	core	sympl.	incl.	incl.	sympl.
SiO_2	38·40	38·11	50·92	49·15	48·89	50·61	51·33	51·39	50·13	50·39	49·70	50·83	40·34	40·41	41·33	37·35	53·57	43·52
TiO_2	0·13	0·07	0·31	0·52	0·53	0·22	0·17	0·18	0·16	0·22	0·16	0·06	2·80	1·91	1·11	5·02	0·04	—
Al_2O_3	21·48	21·07	2·36	3·61	3·90	2·17	1·75	1·77	2·10	2·20	2·46	1·19	12·80	13·25	12·04	13·83	28·73	35·05
Cr_2O_3	0·07	—	0·09	0·02	—	0·06	0·08	—	0·03	—	—	0·02	0·09	0·03	0·05	—	—	—
Fe_2O_3	0·55	—	3·03	2·37	4·21	2·63	2·12	0·42	1·98	1·60	0·58	2·01	1·00	0·84	3·81	1·62	—	—
FeO	26·48	28·83	8·79	12·09	9·49	9·82	10·54	26·63	27·42	28·13	28·96	28·26	13·22	14·07	12·15	11·12	0·24	0·42
MnO	0·78	1·85	0·16	0·20	0·15	0·21	0·22	0·27	0·43	0·49	0·31	0·45	0·04	0·04	0·15	0·05	—	—
MgO	5·83	3·36	13·15	11·67	11·45	12·11	12·2	19·09	17·23	17·11	16·42	17·43	11·44	10·72	11·63	16·59	0·05	—
CaO	6·60	6·88	21·84	19·73	21·31	22·27	22·1	0·54	1·12	0·86	0·82	0·60	11·94	11·89	12·16	0·03	12·43	19·78
Na_2O	—	0·02	0·16	0·18	0·25	0·12	0·15	—	0·02	0·05	—	0·06	1·45	1·56	1·05	0·26	4·35	0·31
K_2O	—	—	0·02	0·01	0·01	—	—	—	—	—	—	—	2·46	2·39	2·99	9·84	0·20	0·02
Total	100·32	100·19	100·83	99·55	100·19	100·22	100·66	100·29	100·62	101·05	99·41	100·71	97·58	97·11	98·47	95·71	99·61	99·10
O cations	12	12	6	6	6	6	6	6	6	6	6	6	23	23	23	11	8	8
Si	2·987	3·016	1·902	1·877	1·853	1·912	1·931	1·949	1·920	1·923	1·930	1·945	6·077	6·128	6·191	2·766	2·436	2·038
Ti	0·008	0·004	0·009	0·015	0·015	0·006	0·005	0·005	0·005	0·006	0·005	0·002	0·317	0·218	0·125	0·280	0·001	—
Al	1·968	1·964	0·104	0·162	0·174	0·097	0·078	0·079	0·095	0·099	0·113	0·054	2·273	2·369	2·126	1·206	1·538	1·933
Cr	0·004	—	0·003	0·001	—	0·002	0·002	—	0·001	—	—	0·001	0·011	0·004	0·006	—	—	—
Fe^{3+}	0·032	—	0·085	0·068	0·108	0·075	0·06	0·012	0·057	0·046	0·017	0·058	0·113	0·096	0·429	0·090	—	—
Fe^{2+}	1·723	1·908	0·274	0·386	0·313	0·311	0·332	0·845	0·878	0·898	0·940	0·904	1·666	1·785	1·521	0·688	0·009	0·016
Mn	0·051	0·124	0·005	0·006	0·005	0·007	0·007	0·009	0·014	0·016	0·010	0·015	0·005	0·005	0·019	0·003	—	—
Mg	0·676	0·396	0·732	0·664	0·647	0·682	0·684	1·079	0·983	0·973	0·950	0·994	2·569	2·423	2·596	1·831	0·003	—
Ca	0·550	0·583	0·874	0·807	0·866	0·901	0·891	0·022	0·046	0·035	0·034	0·025	1·927	1·932	1·952	0·002	0·606	0·992
Na	—	0·003	0·012	0·013	0·009	0·009	0·011	—	0·001	0·004	—	0·004	0·424	0·459	0·305	0·037	0·384	0·028
K	—	—	0·001	—	—	—	—	—	—	—	—	—	0·473	0·462	0·571	0·930	0·012	0·001
X_{Mg}	0·28	0·17	0·73	0·63	0·67	0·69	0·67	0·56	0·53	0·52	0·50	0·52	0·61	0·58	0·63	0·73		

	80-2 (mafic granulite)																		
Mineral:	Grt	Grt	Cpx	Cpx	Cpx	Cpx	Opx	Opx	Opx	Opx	Opx	Amp	Amp	Amp	Pl	Pl	Pl	Pl
Domain:	Core	rim	incl.	reint.	core	rim	incl.	reint.	core	lam.	sympl.	incl.	core	sympl.	incl.	core	rim	sympl.
SiO_2	38·10	37·68	50·30	49·63	49·58	50·45	51·55	50·39	50·79	49·93	50·77	40·91	40·48	41·40	53·95	54·02	45·12	43·10
TiO_2	0·08	—	0·80	0·49	0·55	0·20	0·10	0·15	0·11	0·06	0·04	2·51	2·33	1·41	0·01	—	—	—
Al_2O_3	21·48	21·18	2·81	3·47	3·91	2·31	1·36	1·29	1·43	2·29	1·14	12·86	12·44	11·86	28·97	28·76	34·84	35·03
Cr_2O_3	0·03	0·08	—	0·03	0·04	0·03	0·04	0·02	—	0·020	0·07	0·02	0·11	0·06	—	—	0·04	—
Fe_2O_3	0·92	0·76	2·55	2·24	1·93	1·81	0·07	0·10	—	0·960	—	1·28	1·15	2·50	—	—	—	—
FeO	25·61	27·32	9·72	13·65	11·58	11·49	28·06	30·01	29·73	30·87	29·83	12·40	15·48	14·12	0·40	0·24	0·33	0·57
MnO	1·34	2·26	0·31	0·35	0·31	0·34	0·51	0·64	0·65	0·48	0·73	0·13	0·17	0·10	0·03	0·02	—	0·06
MgO	5·65	3·48	12·38	11·06	10·53	11·35	18·12	15·82	16·04	15·31	16·23	11·79	9·90	10·80	0·03	0·03	0·06	0·01
CaO	6·78	7·04	21·58	19·52	21·74	21·43	0·68	1·10	1·00	0·86	0·66	11·77	11·60	11·63	11·91	11·89	19·18	19·63
Na_2O	—	0·06	0·24	0·23	0·27	0·21	—	0·03	0·060	—	—	1·80	1·89	1·69	4·23	4·77	0·79	0·55
K_2O	—	—	—	—	—	—	—	—	0·010	—	0·01	1·89	1·85	2·11	0·32	0·41	0·03	0·02
Total	99·99	99·86	100·69	100·67	100·44	99·62	100·49	99·55	99·82	100·78	99·48	97·36	97·40	97·68	99·85	100·14	100·39	98·97
O cations	12	12	6	6	6	6	6	6	6	6	6	23	23	23	8	8	8	8

(continued)

Table 1: Continued

	80-2 (mafic granulite)																	
Mineral:	Grt	Grt	Cpx	Cpx	Cpx	Cpx	Opx	Opx	Opx	Opx	Opx	Amp	Amp	Amp	Pl	Pl	Pl	Pl
Domain:	Core	rim	incl.	reint.	core	rim	incl.	reint.	core	lam.	sympl.	incl.	core	sympl.	incl.	core	rim	sympl.
Si	2·976	2·988	1·888	1·884	1·879	1·924	1·965	1·965	1·971	1·932	1·978	6·133	6·158	6·255	2·444	2·445	2·079	2·025
Ti	0·005	—	0·023	0·014	0·016	0·006	0·003	0·004	0·003	0·002	0·001	0·283	0·267	0·160	—	—	—	—
Al	1·976	1·979	0·124	0·155	0·175	0·104	0·061	0·059	0·065	0·104	0·052	2·273	2·231	2·113	1·545	1·533	1·891	1·938
Cr	0·002	0·005	—	0·001	0·001	0·001	0·001	0·001	—	0·001	0·002	0·002	0·013	0·007	—	—	0·001	—
Fe^{3+}	0·054	0·043	0·072	0·064	0·055	0·052	0·002	0·003	—	0·028	—	0·144	0·132	0·284	—	—	—	—
Fe^{2+}	1·673	1·714	0·305	0·433	0·367	0·367	0·894	0·978	0·965	0·999	0·972	1·555	1·970	1·784	0·015	0·009	0·013	0·022
Mn	0·089	0·152	0·010	0·011	0·010	0·011	0·016	0·021	0·021	0·016	0·024	0·017	0·022	0·011	0·001	0·001	—	0·002
Mg	0·658	0·411	0·693	0·626	0·595	0·645	1·029	0·919	0·928	0·883	0·942	2·634	2·245	2·432	0·002	0·002	0·004	0·001
Ca	0·567	0·598	0·868	0·794	0·883	0·876	0·028	0·046	0·042	0·036	0·028	1·891	1·891	1·883	0·578	0·576	0·947	0·988
Na	—	0·009	0·017	0·017	0·020	0·016	—	0·002	0·005	—	—	0·523	0·558	0·495	0·372	0·419	0·071	0·050
K	—	—	—	—	—	—	—	—	—	—	—	0·361	0·359	0·407	0·013	0·024	0·002	0·001
X_{Mg}	0·28	0·19	0·69	0·59	0·62	0·64	0·54	0·48	0·49	0·47	0·49	0·63	0·53	0·58				

	70-22 (paragneiss)											72-7 (orthogneiss)							
Mineral:	Grt	Grt	Grt	Opx	Opx	Bt	Bt	Bt	Ms	Pl	Pl	Grt	Grt	Opx	Opx	Bt	Bt	Bt	Pl	Pl
Domain:	core	rim1	rim2	core	rim	incl.	core	rim	incl.	core	rim	core	rim	core	rim	incl.	core	rim	core	rim
SiO_2	38·97	38·47	37·61	49·46	50·47	37·65	37·56	37·84	42·58	56·97	56·20	37·24	38·01	49·74	51·39	38·06	37·56	37·76	56·53	55·57
TiO_2	0·03	0·03	—	0·07	0·10	5·53	4·53	4·48	0·09	0·04	0·07	0·03	—	0·14	0·12	5·09	2·91	2·51	0·02	—
Al_2O_3	21·81	21·68	21·49	4·86	4·68	14·50	14·84	14·89	13·16	27·16	27·53	21·63	20·96	2·18	1·32	14·58	14·80	14·95	27·30	28·00
Cr_2O_3	—	0·02	0·03	0·09	0·13	0·16	0·10	0·12	0·03	—	—	—	0·04	0·03	—	0·03	0·02	0·01	—	0·06
Fe_2O_3	0·22	—	—	3·13	2·53	1·43	1·63	1·70	—	—	—	1·65	0·45	1·03	—	1·89	2·18	2·16	—	—
FeO	26·54	27·80	32·17	23·07	20·87	9·82	11·26	11·72	5·70	0·12	0·18	27·83	30·53	29·44	29·34	12·93	14·96	14·76	0·08	0·13
MnO	1·94	2·27	2·50	0·55	0·43	0·02	0·02	0·05	0·05	0·08	0·02	2·10	2·50	0·65	0·70	0·05	0·06	0·08	—	—
MgO	8·21	7·63	4·57	19·83	21·91	16·44	15·51	15·84	24·14	0·02	—	5·64	4·65	16·30	16·08	15·19	14·38	14·98	0·04	0·02
CaO	2·79	1·78	1·64	0·11	0·08	0·04	—	—	—	9·76	10·03	3·62	3·27	0·37	0·30	0·01	0·02	0·08	9·60	10·31
Na_2O	—	0·02	0·01	0·02	—	0·05	—	—	0·03	5·82	5·55	—	—	—	—	0·15	—	0·16	6·15	6·18
K_2O	—	—	—	—	—	10·18	10·12	10·23	10·16	0·47	0·44	—	—	—	0·01	9·49	9·82	8·62	0·24	0·19
Total	100·51	99·70	100·02	101·19	101·20	95·82	95·57	96·87	95·94	100·44	100·02	99·74	100·41	99·88	99·26	97·47	96·71	96·07	99·96	100·46
O cations	12	12	12	6	6	11	11	11	11	8	8	12	12	6	6	11	11	11	8	8
Si	3·000	3·002	2·992	1·847	1·859	2·764	2·782	2·772	3·004	2·552	2·529	2·941	3·006	1·930	2·006	2·778	2·799	2·809	2·542	2·498
Ti	0·002	0·002	—	0·002	0·003	0·305	0·252	0·247	0·005	0·001	0·002	0·002	—	0·004	0·004	0·279	0·163	0·140	0·001	—
Al	1·977	1·992	2·006	0·214	0·203	1·253	1·294	1·285	1·093	1·433	1·459	2·011	1·952	0·100	0·061	1·253	1·299	1·310	1·446	1·482
Cr	—	0·001	0·002	0·003	0·004	0·009	0·006	0·007	0·002	—	—	—	0·002	0·001	—	0·002	0·001	0·001	—	—
Fe^{3+}	0·013	—	—	0·088	0·070	0·079	0·091	0·094	—	—	—	0·098	0·027	0·030	—	0·104	0·122	0·121	—	—
Fe^{2+}	1·709	1·814	2·140	0·721	0·642	0·603	0·697	0·718	0·336	0·004	0·007	1·838	2·019	0·955	0·958	0·789	0·932	0·918	0·003	0·005
Mn	0·127	0·150	0·168	0·017	0·013	0·001	0·001	0·003	0·003	0·003	0·001	0·140	0·167	0·021	0·023	0·003	0·004	0·005	—	—
Mg	0·942	0·887	0·542	1·103	1·202	1·799	1·712	1·730	2·539	0·001	—	0·664	0·548	0·943	0·936	1·653	1·597	1·661	0·003	0·001
Ca	0·230	0·149	0·140	0·004	0·003	0·003	—	—	—	0·468	0·484	0·306	0·277	0·015	0·013	0·001	0·002	0·006	0·463	0·497
Na	—	0·003	0·002	0·001	—	0·007	—	—	0·004	0·505	0·484	—	—	—	—	0·021	—	0·023	0·536	0·539
K	—	—	—	—	—	0·953	0·956	0·956	0·914	0·027	0·025	—	—	—	0·000	0·884	0·934	0·818	0·014	0·011
X_{Mg}	0·36	0·33	0·20	0·60	0·65	0·75	0·71	0·71	0·88			0·27	0·21	0·50	0·49	0·68	0·63	0·64		

—, not detectable. $X_{Mg} = Mg/(Mg + Fe^{2+})$. Mineral abbreviations are after Kretz (1983) except for amphibole (Amp).

The quoted errors in isochron ages represent two standard deviations (2σ). Sm–Nd model ages (T_{DM}) were calculated in two ways. The one-stage model age (T_{DM^1}) is calculated assuming a linear isotopic evolution of the depleted mantle reservoir from $\varepsilon_{Nd}(T) = 0$ at 4·56 Ga to +10 at the present. The two-stage model age (T_{DM^2}) is obtained assuming that the protolith of the granitic magmas has the Sm/Nd ratio of the average continental crust (Keto & Jacobsen, 1987). Nd isotopic normalization parameters used for the calculation of model ages are the same as those of Liu *et al.* (2006).

PETROLOGY AND THERMOBAROMETRY

Mineral assemblages and textures

Mafic granulites

Mafic granulites are composed of garnet, clinopyroxene, orthopyroxene, amphibole, intergrown magnetite–ilmenite, apatite and zircon, with or without plagioclase. These minerals (except the accessory phases) form coarse-grained (1–2 mm), near-equigranular textures (Fig. 4a), and are inferred to have equilibrated at peak metamorphic conditions. The mafic granulites can be divided into two subtypes. Type I granulites (samples 70-11 and 80-11) have higher modal abundances of garnet (25–40%), greater modal clinopyroxene than orthopyroxene, and no preserved plagioclase. Type II granulites (samples 80-1, 80-2 and 80-6) contain plagioclase, less garnet (5–10%) and less modal clinopyroxene relative to orthopyroxene. Early amphibole in both subtypes is minor (<5%) and appears in textural equilibrium with the other phases. Garnet contains inclusions of clinopyroxene, orthopyroxene, amphibole, plagioclase (with the exception of sample 70-11), quartz, intergrown magnetite–ilmenite, apatite and less commonly biotite (Fig. 4a). The suite of minerals occurring as inclusions in garnet is very similar to that in the matrix. The exception is quartz, which, although present in garnet, is absent from the matrix. Zircon is observed either as intergranular grains or as inclusions in other minerals.

In all mafic granulites, garnet porphyroblasts, especially when in contact with clinopyroxene, are partially replaced by fine-grained, radial and vermicular symplectites. The symplectites are typically composed of orthopyroxene and plagioclase, with or without trace amounts of clinopyroxene, amphibole and intergrown magnetite–ilmenite (Fig. 4b and c). These textures are interpreted to have resulted from the following two reactions (Harley, 1988; Thost *et al.*, 1991):

$$\underset{\text{Grt}}{\text{Ca(Fe,Mg)}_2\text{Al}_2\text{Si}_3\text{O}_{12}} + \underset{\text{Qtz}}{\text{SiO}_2} = \underset{\text{Opx}}{\text{(Fe,Mg)}_2\text{Si}_2\text{O}_6} + \underset{\text{Pl}}{\text{CaAl}_2\text{Si}_2\text{O}_8} \quad (1)$$

$$\underset{\text{Grt}}{\text{Ca(Fe,Mg)}_2\text{Al}_2\text{Si}_3\text{O}_{12}} + \underset{\text{Cpx}}{\text{Ca(Fe,Mg)Si}_2\text{O}_6} + \underset{\text{Qtz}}{\text{SiO}_2} = 2\underset{\text{Opx}}{\text{(Fe,Mg)}_2\text{Si}_2\text{O}_6} + \underset{\text{Pl}}{\text{CaAl}_2\text{Si}_2\text{O}_8}. \quad (2)$$

Garnet is inferred to have been completely resorbed where domains of symplectic orthopyroxene, clinopyroxene, plagioclase and/or amphibole occur (Fig. 4d). Plagioclase has commonly recrystallized to form optically continuous grains. However, backscattered electron (BSE) images show that some of them have dark, inclusion-free cores, which may represent the relics of primary plagioclase (Fig. 4e). In addition, large amphibole grains that enclose all the peak minerals and symplectites are commonly developed (Fig. 4f). These amphiboles, together with some large biotite flakes, are weakly aligned parallel to the regional gneissosity, suggesting that the rocks underwent recrystallization during retrograde metamorphism.

Coarse matrix clinopyroxene contains two sets of orthopyroxene lamellae exsolved parallel to the (100) and (001) planes of the host crystals (Fig. 4g and h). Lamellae parallel to (100) planes are long, relatively coarse (maximum up to 2 μm wide) and closely spaced, whereas lamellae parallel to the (001) planes are short (<20 μm in length), narrow (mostly <0·5 μm wide), and very rare. The (100) lamellae are commonly contiguous to symplectic orthopyroxene mantling garnet (see Fig. 4c). Rare Fe–Ti oxide rods usually occur accompanying the orthopyroxene exsolution (Fig. 4h). Coarse matrix orthopyroxene contains very narrow exsolution lamellae (*c.* 0·2 μm wide) of clinopyroxene as well as Fe–Ti oxides (Fig. 4i and j). Both lamellae minerals can occur on the same (100) plane of the host orthopyroxene. Lamellae of Fe–Ti oxide are discontinuous and occur as parallelogram-like plates 20–80 μm in length and 0·5–1 μm in width.

Felsic paragneisses and orthogneisses

Felsic para- and orthogneisses both contain garnet, orthopyroxene, biotite, plagioclase, K-feldspar, quartz, intergrown magnetite–ilmenite, apatite and zircon, with or without spinel and monazite (Fig. 4k). Paragneisses are distinguished from orthogneisses by having higher modes of garnet (8–20%), orthopyroxene (10–25%) and biotite (mostly >5%) and lower modes of K-feldspar (<2%). Garnet is hypidiomorphic or, in some cases, xenomorphic, with grain sizes ranging from 0·5 to 5 mm. Most garnets contain numerous inclusions of biotite, plagioclase, quartz and intergrowths of magnetite, ilmenite and/or spinel. In sample 70-22, muscovite, which appears to be in textural equilibrium with biotite, plagioclase and quartz, is also observed as inclusions in garnet (Fig. 4l). Orthopyroxene is hypidiomorphic or xenomorphic and may contain inclusions of biotite, plagioclase and quartz. As in the mafic granulites, rare Fe–Ti oxide lamellae are

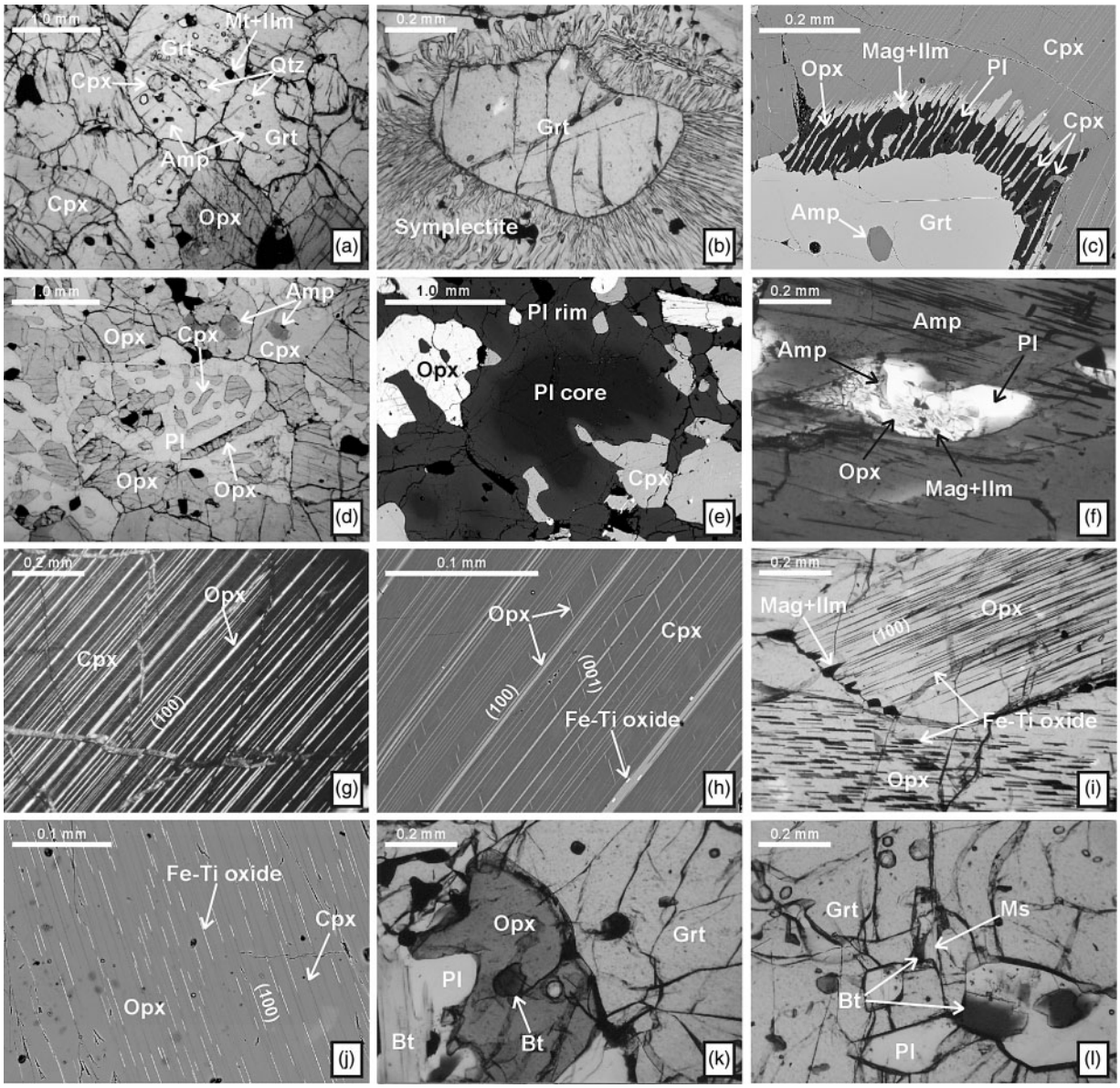

Fig. 4. Photomicrographs and backscattered electron images showing the textures and mineral parageneses in mafic granulites and felsic gneisses from the McKaskle Hills. (a) Matrix assemblage of granoblastic, near-equigranular garnet + clinopyroxene + orthopyroxene from a mafic granulite [sample 70-1l; plane-polarized light (PPL) photomicrograph]. Quartz, clinopyroxene, amphibole and magnetite–ilmenite occur as inclusions in garnet. (b) Fine-grained vermicular symplectite around embayed garnet from a mafic granulite (sample 80-6; PPL photomicrograph). (c) Symplectic orthopyroxene + plagioclase separating garnet from clinopyroxene in mafic granulite (sample 80-1; BSE image). (d) Symplectic orthopyroxene + clinopyroxene + plagioclase as a pseudomorph after garnet from a mafic granulite (sample 70-1l; PPL photomicrograph). (e) A plagioclase grain with a dark, Ca-poor core and a bright, Ca-rich rim from mafic granulite (sample 80-2; BSE image). (f) A large amphibole grain enclosing a symplectite of orthopyroxene + amphibole + plagioclase + magnetite–ilmenite (sample 80-6; PPL photomicrograph). (g) Clinopyroxene containing closely spaced orthopyroxene lamellae aligned in the (100) plane from mafic granulite (sample 80-2; cross-polarized light photomicrograph). (h) Two sets of orthopyroxene lamellae inferred to have exsolved parallel to the (100) and (001) planes of the host clinopyroxene from a mafic granulite (sample 80-2; BSE image). (i) Orthopyroxene containing thin, parallelogram lamellae of Fe–Ti oxide from a mafic granulite (sample 80-6; PPL photomicrograph). (j) Very narrow exsolution lamellae of both Fe–Ti oxide and clinopyroxene in orthopyroxene from mafic granulite (sample 80-6; BSE image). (k) Paragenesis of garnet + orthopyroxene + biotite + plagioclase from paragneiss (sample 70-22; PPL photomicrograph). (l) Muscovite + biotite + plagioclase inclusions in garnet from paragneiss (sample 70-22; PPL photomicrograph).

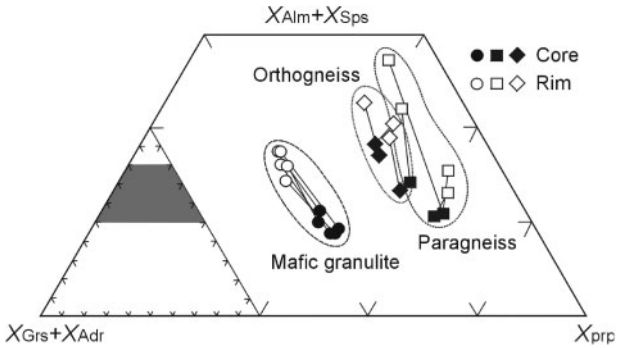

Fig. 5. Ternary $(X_{Alm}+X_{Sps})$–$(X_{Grs}+X_{Adr})$–X_{Prp} diagram illustrating the chemical compositions of garnet from mafic granulites and felsic gneisses

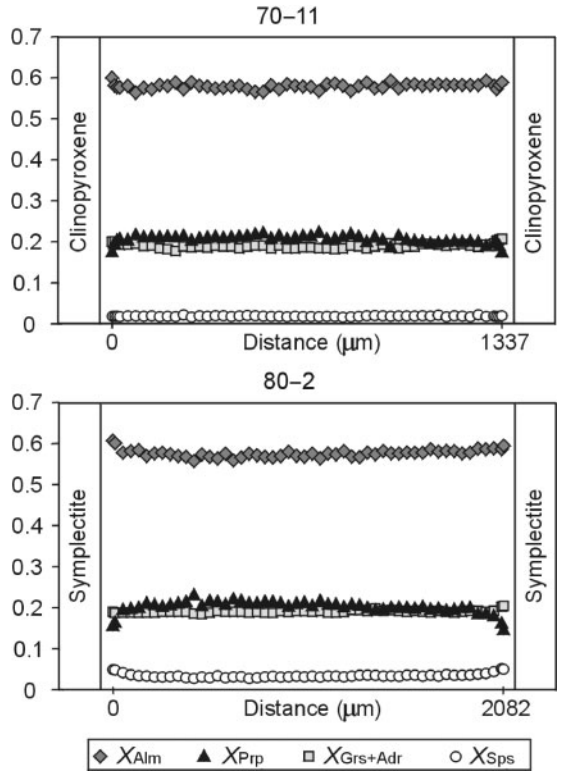

Fig. 6. Representative compositional zoning profiles across garnet from mafic granulites.

exsolved from orthopyroxene. Spinel occurs in some samples (70-22, 71-7 and 74-5), occurring as blebs or blades within magnetite–ilmenite intergrowths. K-feldspar commonly contains numerous exsolved blebs of albite. In paragneiss samples, late K-feldspar is locally developed along fractures in plagioclase or in intergranular fractures. Vermicular symplectites of quartz and plagioclase also occur around relict biotite or K-feldspar. These might reflect the products of partial melting at or near peak metamorphism.

Mineral compositions

The end-members of garnet were calculated after the scheme of Deer *et al.* (1992). Garnet in the mafic granulites consists predominantly of almandine (X_{Alm} 0·56–0·58), pyrope (X_{Prp} 0·20–0·23) and grossular (X_{Grs} 0·14–0·20), with minor spessartine (X_{Sps} 0·02–0·03) and andradite (X_{Adr} 0·00–0·05) (Fig. 5). Garnet is not significantly zoned in X_{Alm}, X_{Prp}, X_{Grs} and X_{Sps}, being characterized by flat profiles across much of a grain, decreasing in X_{Prp} (0·13–0·15) and increasing in X_{Alm} (0·61–0·63) and X_{Sps} (0·04–0·05) within 25–50 μm of the rim when in contact with clinopyroxene or symplectite (Fig. 6). Garnet from felsic para- and orthogneisses is dominated by X_{Alm} (0·57–0·65) and X_{Prp} (0·21–0·31), with minor X_{Grs} (0·07–0·10), X_{Sps} (0·03–0·05) and X_{Adr} (0·00–0·02). Generally, garnet from paragneisses is more magnesian than that from orthogneisses. Garnet from both of these rock types shows compositional zoning with decreasing X_{Prp} and X_{Grs} and increasing X_{Alm} and X_{Sps} from core to rim (Fig. 5). This zoning is more pronounced when garnet is in contact with another ferromagnesian mineral, indicating significant Fe–Mg resetting during cooling.

The end-members of clinopyroxene were normalized based on wollastonite $(Wo) = Ca/(Ca + Mg + Fe^{2+})$, enstatite $(En) = Ca/(Ca + Mg + Fe^{2+})$, and ferrosilite $(Fs) = Ca/(Ca + Mg + Fe^{2+})$. Clinopyroxene from mafic granulites has compositions in the range of 43–49 mol % Wo, 32–39 mol % En and 15–23 mol % Fs. It contains 1·7–3·9 wt % Al_2O_3 and X_{Mg} $[=Mg/(Mg + Fe^{2+})]$ ranges from 0·59 to 0·73. Clinopyroxene compositions vary with textural position. Within individual samples, the reintegrated matrix clinopyroxene has a lower concentration of Ca, a higher concentration of Al and a lower X_{Mg} when compared with clinopyroxene inclusions in garnet and the symplectic clinopyroxene or clinopyroxene rim adjacent to symplectic orthopyroxene and plagioclase.

Orthopyroxene in the mafic granulites has 1·0–2·5 wt % Al_2O_3 and X_{Mg} ranges from 0·46 to 0·54. Similar to clinopyroxene, orthopyroxene compositions vary with textural position. Generally, the symplectic orthopyroxene has lower Al and Ca contents, whereas orthopyroxene inclusions in garnet have lower Ca contents and X_{Mg} relative to the reintegrated matrix orthopyroxene. Orthopyroxene from felsic para- and orthogneisses has 1·3–4·7 wt % Al_2O_3 and X_{Mg} ranges from 0·46 to 0·65. Orthopyroxene in the paragneisses commonly has a higher X_{Mg} and Al content than that from the orthogneisses. Individual orthopyroxene grains typically show a decrease of Al and Ca and an increase of X_{Mg} from core to rim.

Amphibole in mafic granulites is pargasitic ($Ca_B > 1·8$; $Na_A + K_A > 0·7$; $Ti < 0·4$; $Si = 6·07–6·28$ p.f.u.) with X_{Mg}

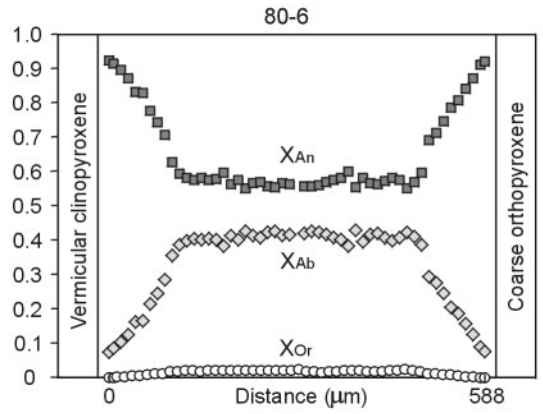

Fig. 7. Representative compositional zoning profile for plagioclase from mafic granulite 80-6.

ranging from 0·53 to 0·64. Amphibole inclusions in garnet have relatively high X_{Mg}, whereas the large retrograde amphibole grains have a lower X_{Mg}. The X_{Mg} of amphibole in the matrix and symplectites is variable. Nevertheless, within a single sample, amphibole in symplectites exhibits both higher Si content and X_{Mg} when compared with amphibole in the matrix.

Biotite inclusions in garnet in mafic granulites have TiO_2 contents of 1·9–5·0 wt % and X_{Mg} of 0·73–0·81. Retrograde biotite has X_{Mg} of 0·66–0·69 and a nearly constant TiO_2 content of 4·2–4·4 wt %. For felsic para- and orthogneisses, biotite in different samples has variable TiO_2 contents (2·5–7·8 wt %) and X_{Mg} (0·56–0·78). However, within a given sample, biotite inclusions in garnet have higher TiO_2 contents and X_{Mg} compared with matrix biotite. No significant core-to-rim variation in composition was observed for matrix biotite grains. Inclusions of muscovite in garnet from paragneiss sample 70-22 show little compositional variation. The Si values range from 3·93 to 3·00 p.f.u., and X_{Mg} values from 0·86 to 0·88.

The end-members of plagioclase were normalized based on anorthite (An) = Ca/(Ca + Na) and albite (Ab) = Na/(Ca + Na). Plagioclase from mafic granulites has dominantly labradorite and anorthite compositions depending on textural position. Matrix plagioclase exhibits pronounced compositional zoning, with a homogeneous core (X_{An} 0·55–0·62) and a distinctly anorthitic rim (X_{An} 0·90–0·95) (Fig. 7). Plagioclase inclusions in garnet have X_{An} of 0·60–0·62, similar to the core compositions observed for matrix plagioclase. However, within individual samples, inclusion plagioclases may have slightly higher X_{An} than matrix plagioclase cores. Symplectic plagioclase has the highest X_{An} (0·95–0·97). Plagioclase from felsic para- and orthogneisses is andesine to labradorite in composition (X_{An} 0·36–0·57). Most grains display slight compositional zoning with a rimward enrichment in Ca of less than $X_{An} = 0·04$.

Thermobarometry and *P–T* path

To evaluate *P–T* conditions for the different stages of granulite-facies metamorphism in the McKaskle Hills, we employ average *P–T* calculations using THERMOCALC and thermobarometry based on the retrieval technique. Average *P–T* calculations followed the method of Powell & Holland (1994), using an updated and expanded version of the internally consistent thermodynamic dataset (Holland & Powell, 1998) and the software THERMOCALC 3.1. The activities for end-members in garnet, clinopyroxene, orthopyroxene, amphibole, biotite, plagioclase and K-feldspar were calculated using the software AX (Holland, available at http://www.esc.cam.ac.uk/astaff/holland/index.html). The fluid phase was assumed to be an H_2O-bearing mixture. The convergence method for the recovery of peak metamorphic *P–T* conditions (Fitzsimons & Harley, 1994*b*; Pattison & Bégin, 1994) adjusts Fe–Mg ratios in both garnet and orthopyroxene until the temperature estimates using a Fe–Mg exchange thermometer (e.g. Harley, 1984) and an Al-solubility thermometer (e.g. Harley & Green, 1982) converge. This technique has been successfully used on other granulite terranes (e.g. Bégin & Pattison, 1994; Chacko *et al.*, 1996; Jones & Escher, 2002). Here we employ the RCLC program (Pattison *et al.*, 2003) which uses the TWQ 2.02b thermodynamic dataset (Berman & Aranovich, 1996) with modifications to incorporate the experiments of Aranovich & Berman (1997) on Al solubility of orthopyroxene.

The results of average *P–T* calculations using THERMOCALC for mafic granulites and felsic gneisses are given in Table 2, and a comparison of uncorrected Fe–Mg, uncorrected Fe–Al and corrected Fe–Mg–Al *P–T* estimates using RCLC given in Table 3. The core compositions of garnet, amphibole and plagioclase and the reintegrated compositions of clino- and orthopyroxenes for mafic granulites yield average *P–T* estimates of 883–948°C and 9·0–9·5 kbar for the peak stage, whereas the rim compositions of garnet together with symplectic clinopyroxene (or clinopyroxene rim) + orthopyroxene + amphibole + plagioclase yield average *P–T* estimates of 710–736°C and 6·4–7·3 kbar for the retrograde stage. In contrast, the corrected Fe–Mg–Al *P–T* estimates from garnet–orthopyroxene pairs are 763–902°C and 8·3–10·6 kbar for the peak stage, and 698–748°C and 6·6–7·2 kbar for the retrograde stage. The corrected Fe–Mg–Al *P–T* estimates for the retrograde stage are equivalent to those determined using THERMOCALC, but both retrieval temperatures and pressures for the peak stage (except for sample 80-6) are significantly lower than the THERMOCALC average *P–T* estimates. As usual, the uncorrected Fe–Mg temperatures are successively lower than the uncorrected Fe–Al and corrected Fe–Mg–Al temperatures, consistent with more rapid diffusion of Fe–Mg vs Al

Table 2: Average P–T *estimates for mafic granulites and felsic gneisses using THERMOCALC*

Sample	T (°C)	P (kbar)	aH_2O	Correl.	Fit	*NR*
Mafic granulite						
Matrix assemblage						
80-1	948 ± 68	9·5 ± 1·6	0·4	0·544	0·89	10
80-2	923 ± 64	9·0 ± 1·5	0·3	0·525	0·84	10
80-6	883 ± 57	9·3 ± 1·5	0·4	0·515	0·88	10
Symplectite assemblage						
70-11	710 ± 83	7·3 ± 2·5	0·1	0·512	2·03	8
80-11	721 ± 72	7·0 ± 2·1	0·1	0·514	1·65	8
80-1	714 ± 68	6·6 ± 1·9	0·2	0·533	1·56	9
80-2	732 ± 50	6·4 ± 1·3	0·2	0·491	1·07	10
80-6	736 ± 57	7·0 ± 1·7	0·2	0·452	1·42	9
Felsic gneiss						
70-6	880 ± 57	7·9 ± 1·4	0·2	0·484	0·83	5
70-22	741 ± 31	7·7 ± 1·2	0·1	0·381	0·53	6
71-7	877 ± 43	7·7 ± 1·3	0·3	0·435	0·84	6
72-7	698 ± 32	5·9 ± 1·1	0·1	0·460	0·34	6
74-5	796 ± 41	7·2 ± 1·2	0·2	0·459	0·66	6
78-5	796 ± 43	6·9 ± 1·2	0·2	0·440	0·55	5

aH_2O, fluid composition used; Correl., correlation between the uncertaintiess on *P* and *T*; Fit, a goodness of fit parameter describing the average of *n* equilibria (Powell & Holland, 1988); *NR*, the number of independent equilibria calculated by THERMOCALC.

Table 3: Retrieval P–T *estimates for mafic granulites and felsic gneisses using RCLC*

Sample	Uncorrected Fe–Mg		Uncorrected Fe–Al		Corrected Fe–Mg–Al	
	T (°C)	*P* (kbar)	*T* (°C)	*P* (kbar)	*T* (°C)	*P* (kbar)
Mafic granulite						
Matrix assemblage						
80-1	914	8·9	807	8·4	770	8·3
80-2	1028	11·5	829	8·6	763	8·5
80-6	889	10·4	896	10·6	902	10·6
Symplectite assemblage						
70-11	633	6·4	705	7·3	740	7·2
80-11	589	5·6	695	6·8	741	6·7
80-1	634	5·8	713	6·7	744	6·6
80-2	707	6·4	737	6·7	748	6·7
80-6	646	6·2	683	6·6	698	6·6
Felsic gneiss						
70-6	791	7·7	809	7·9	816	7·9
70-22	725	7·6	898	10·0	979	10·1
71-7	906	8·9	903	8·8	902	8·8
72-7	802	7·6	822	7·9	829	7·9
74-5	848	8·1	874	8·4	884	8·4
78-5	910	9·0	901	8·8	898	8·8

(Fitzsimons & Harley, 1994*b*; Pattison & Bégin, 1994). However, as many mafic granulites from other areas have shown (Pattison *et al.*, 2003), a reverse order for Fe–Mg, Fe–Al and Fe–Mg–Al temperature estimates is given by the peak mineral assemblages of samples 80-1 and 80-2. The reason for this unreasonable pattern is unclear, but thermodynamic inaccuracy is the most likely single explanation (Pattison *et al.*, 2003).

Because no retrograde reaction textures occur in the felsic gneisses we can only estimate the peak *P–T* conditions for the rocks. The average *P–T* estimates using the core compositions of garnet + orthopyroxene + biotite + plagioclase + K-feldspar + quartz are 698–880°C and 5·9–7·9 kbar, whereas the corrected Fe–Mg–Al *P–T* estimates are 816–979°C and 7·9–10·1 kbar. In contrast to the peak *P–T* conditions obtained for mafic granulites, the temperature and pressure estimates for the felsic gneisses determined using THERMOCALC are significantly lower. This suggests that the Fe–Mg compositions of the ferromagnesian minerals used in the THERMOCALC calculations might have been reset during cooling. Furthermore, two samples (70-6 and 72-7) also yield relatively low temperatures and pressures using retrieval thermobarometry.

Considering that the *P–T* results obtained by RCLC are unreasonable for the matrix assemblage of the mafic granulites and slightly scattered for the felsic gneisses, we prefer the average *P–T* conditions of 880–950°C and 9·0–9·5 kbar obtained by THERMOCALC from the matrix assemblage of the mafic granulites as the best estimation of the peak metamorphic conditions in the McKaskle Hills. The pre-peak history is indicated by the preservation of quartz inclusions in garnet in the mafic granulites and muscovite inclusions in garnet in the paragneiss. Although *P–T* conditions for this earlier stage cannot be quantitatively determined as a result of the compositional homogenization of garnet during peak metamorphism, the experimental results suggested that the garnet-in reaction for quartz tholeiites occurred above 7·5–9·0 kbar at 700–800°C (Green & Ringwood, 1967; Rushmer, 1991). The upper stability limit of muscovite is constrained by the muscovite-out reaction, which lies at temperatures not exceeding 650–750°C at 4–9 kbar (Spear *et al.*, 1999; White *et al.*, 2001). The nearly identical *P–T* estimates of about 700–750°C and 6·6–7·2 kbar obtained by both RCLC and

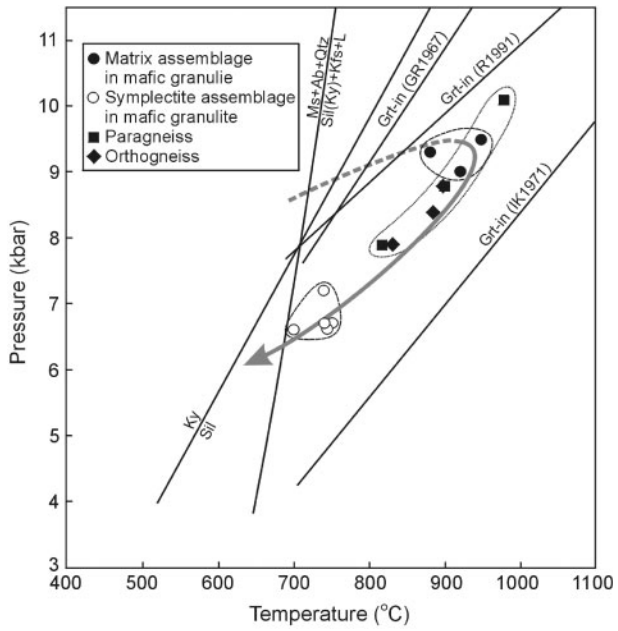

Fig. 8. *P–T* diagram and *P–T* paths of granulites from the McKaskle Hills. *P–T* conditions are estimated using average *P–T* calculations (Powell & Holland, 1994) for the matrix assemblage of mafic granulites and using retrieval *P–T* calculations (Pattison *et al.*, 2003) for felsic gneisses and the symplectite assemblage of mafic granulites. Garnet-in reactions for quartz tholeiite are from Green & Ringwood (1967) and Rushmer (1991), and for olivine basalt from Ito & Kennedy (1971). Reaction curves for Ky = Sil and Ms + Ab + Qtz = Sil (Ky) + Kfs + L are from Salje (1986) and Spear *et al.* (1999), respectively.

THERMOCALC for symplectites place a good constraint on the retrograde conditions for the mafic granulites. Therefore, the post-peak *P–T* trajectory of the granulites from the McKaskle Hills involves a decompression of 2–3 kbar concurrent with cooling of ~ 200°C from the metamorphic peak (Fig. 8).

GEOCHRONOLOGY

SHRIMP U–Pb zircon dating

Sample 80-1: garnet-bearing mafic granulite

Zircons from this sample are colorless or pale yellow and rounded to prismatic in shape, with grain lengths of 70–200 μm. Based on CL images, four distinct domains can be distinguished in these zircon grains. These are banded cores, patchy cores, strongly luminescent rims, and weakly luminescent rims or individual grains. The growth zones in banded cores are broad and straight, and are commonly surrounded by strongly luminescent rims (Fig. 9a). The patchy cores have an extremely low CL response, and in many cases, contain moderately luminescent patches (Fig. 9b and c). Such cores are all embayed by thin or thick, strongly luminescent rims. Amphibole, clinopyroxene, plagioclase and apatite inclusions were observed in both banded and patchy cores. The strongly luminescent rims are commonly homogeneous, but may preserve banded zoning. A more strongly luminescent band commonly occurs on the outer borders of banded or patchy core (Fig. 9a and c). The weakly luminescent rims are very rare, and occur only as overgrowths on banded cores (Fig. 9d). Individual grains, which are nearly isometric and may contain a banded core, are also weakly luminescent, but fir-tree sector zoning is commonly visible in the CL images (Fig. 9e and f).

Forty-seven analyses of 43 zircon grains were obtained on this sample (Table 4 and Fig. 10a). Apart from two analyses (21.1 and 29.1) that are significantly discordant, banded cores yield a very large age range from 1073 ± 45 Ma ($^{207}Pb/^{206}Pb$ age) to 545 ± 15 Ma ($^{206}Pb/^{238}U$ age), with Th/U ratios ranging from 0·36 to 0·73. A group of nine grains form a concordant population with a weighted mean $^{207}Pb/^{206}Pb$ age of 1019 ± 33 Ma (MSWD = 0·45). Other banded cores show younger ages that probably reflect Pb loss related to a subsequent thermal event. The data from strongly luminescent rims are mostly discordant and show large errors on $^{207}Pb/^{206}Pb$ ratios and ages as a result of the small analytical spot size used and the low abundances of U (60–173 ppm) and Th (9–52 ppm). Nearly concordant data from such rims and their enclosed patchy cores give a highly scattered age distribution with a maximum $^{207}Pb/^{206}Pb$ age of 1012 ± 91 Ma and a minimum $^{206}Pb/^{238}U$ age of 503 ± 17 Ma. The data from weakly luminescent rims or individual grains are nearly concordant and grouped, yielding $^{206}Pb/^{238}U$ ages of 561 ± 14 to 500 ± 14 Ma with a mean of 533 ± 9 Ma (n = 15, MSWD = 1·5). Their Th/U ratios are relatively high, ranging from 0·57 to 0·92.

The broad and straight bands preserved in the zircon cores seem not to be a typical feature of magmatic zircons, although similar zoned patterns have been observed in zircon domains from some gabbros (Rubatto & Gebauer, 2000). However, the absence of garnet and orthopyroxene inclusions in the banded domains also precludes their formation by metamorphic overgrowth. Thus, the banded cores are likely to be magmatic in origin, but could have been affected by solid-state recrystallization (Hoskin & Black, 2000). In such a case, the concordia age of 1019 ± 33 Ma obtained for these zircon domains is interpreted to be the minimum emplacement age of the mafic granulite protolith. The fir-tree sector zoning preserved in weakly luminescent zircon rims or individual grains is similar to the inner structure of some granulite-facies zircons (Vavra *et al.*, 1996) and interpreted as the result of metamorphic overgrowth. Therefore, the concordia age of 533 ± 9 Ma obtained for such zircon domains is considered to be the age of the Cambrian metamorphic event. The relatively high Th/U ratios for such zircon domains may have resulted from open-system behaviour, breakdown of high Th/U minerals or competition with high-U

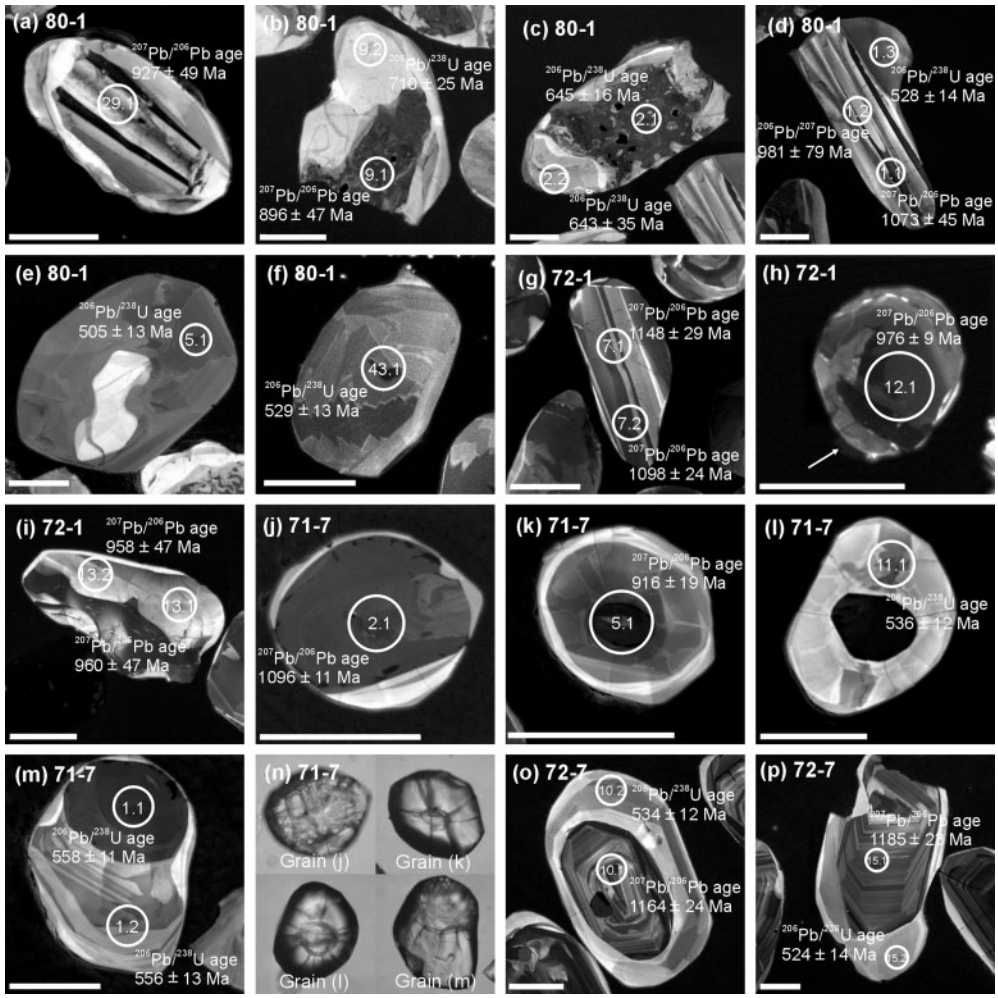

Fig. 9. Representative cathodoluminescence (CL) and transmitted light images of zircons from mafic granulites and felsic gneisses in the McKaskle Hills. (a) Zircon from sample 80-1 showing a banded core surrounded by a strongly luminescent rim. A more strongly luminescent band occurs on the outer border of the zoned core, indicating a recrystallization front. (b) Zircon from sample 80-1 showing a weakly luminescent patchy core embayed by a thick, strongly luminescent rim. (c) Zircon from sample 80-1 showing a patchy core, which contains moderately luminescent patches and numerous amphibole inclusions. A more strongly luminescent band also occurs on the outer border of the patchy core. (d) Zircon from sample 80-1 showing banded zonation with a weakly luminescent overgrowth. (e) Zircon from sample 80-1 showing weakly luminescent domain with a strongly luminescent relict core. Fir-tree sector zoning is visible in the weakly luminescent domain. (f) Zircon from sample 80-1 showing typical fir-tree sector zoning. (g) Zircon from sample 72-1 showing banded zonation. (h) Zircon from sample 72-1 showing thickened banding with an irregular recrystallization domain. A local, weakly luminescent overgrowth is visible (arrow). (i) Zircon from sample 72-1 showing a weakly luminescent core embayed by a thick, moderately luminescent rim. (j) Zircon from sample 71-7 showing a rounded, weakly luminescent core surrounded by a thin, moderately luminescent rim. An oscillatory-zoned domain is preserved in the inner part of the core. (k) Zircon from sample 71-7 showing a rounded, weakly luminescent core surrounded by a weakly luminescent mantle and a thin, moderately luminescent rim. (l) Zircon from sample 71-7 showing a rounded, weakly luminescent core and a thick, fir-tree sector zoned overgrowth. (m) Zircon from sample 71-7 showing a rounded, weakly luminescent core and a thick, banded overgrowth. (n) Transmitted light images of grains (j)–(m) showing well-rounded cores surrounded by overgrowths with numerous radial fractures, clearly indicating a detrital origin for the cores. (o) Zircon from sample 72-7 showing an oscillatory-zoned core surrounded by a moderately luminescent overgrowth. (p) Zircon from sample 72-7 showing an oscillatory-zoned core surrounded by a moderately luminescent overgrowth. Circles with numbers are SHRIMP analytical spots with their identification numbers. Ages are given at 1σ (see Table 4). Scale bars represent 50 μm.

minerals during metamorphism, and cannot be simply regarded as an indicator of a non-metamorphic origin (e.g. Möller *et al.*, 2003).

The preservation of prismatic zircons suggests that the strongly luminescent rims were formed through recrystallization of previously existing zircons rather than as new overgrowths. The more strongly luminescent bands developed near banded or patchy cores could represent recrystallization fronts, as described by Hoskin & Black (2000), whereas the patchy cores could be the modified and disrupted domains of former igneous zircons. Hence, the age data scattered from late Mesoproterozoic to Cambrian

Table 4: SHRIMP U–Pb analyses of zircons from mafic granulites and felsic gneisses from the McKaskle Hills

Spot	U(ppm)	Th (ppm)	Th/U	Pb* (ppm)	Common ^{206}Pb (%)	Isotopic ratios			Ages (Ma)	
						^{206}Pb/^{238}U	^{207}Pb/^{235}U	^{207}Pb/^{206}Pb	^{206}Pb/^{238}U	^{207}Pb/^{206}Pb
Sample 80-1 (garnet-bearing mafic granulite)										
Banded core										
1.1	369	129	0·36	53·5	0·13	0·1688 ± 0·0047	1·749 ± 0·063	0·0752 ± 0·0017	1005 ± 26	1073 ± 45
1.2	231	115	0·52	35·7	0·39	0·1791 ± 0·0122	1·774 ± 0·138	0·0718 ± 0·0028	1062 ± 66	981 ± 79
6.1	193	89	0·48	23·4	1·14	0·1396 ± 0·0042	1·308 ± 0·098	0·0679 ± 0·0047	843 ± 24	866 ± 140
8.1	280	165	0·61	34·6	0·00	0·1435 ± 0·0049	1·424 ± 0·080	0·0720 ± 0·0032	865 ± 27	985 ± 90
11.1	163	86	0·54	20·9	1·42	0·1474 ± 0·0046	1·183 ± 0·111	0·0582 ± 0·0052	886 ± 25	538 ± 190
15.1	300	118	0·40	23·1	1·76	0·0882 ± 0·0026	0·662 ± 0·043	0·0544 ± 0·0032	545 ± 15	389 ± 130
20.1	508	290	0·59	59·2	1·00	0·1343 ± 0·0036	1·214 ± 0·079	0·0656 ± 0·0039	812 ± 21	792 ± 120
21.1	262	144	0·57	20·4	1·16	0·0898 ± 0·0027	0·674 ± 0·056	0·0545 ± 0·0043	554 ± 16	390 ± 170
25.1	353	172	0·50	44·9	0·09	0·1478 ± 0·0041	1·505 ± 0·051	0·0739 ± 0·0014	889 ± 23	1037 ± 39
26.1	302	209	0·72	34·6	0·38	0·1326 ± 0·0036	1·225 ± 0·059	0·0670 ± 0·0027	803 ± 21	838 ± 83
27.1	356	238	0·69	54·4	0·24	0·1773 ± 0·0048	1·773 ± 0·066	0·0726 ± 0·0018	1052 ± 26	1002 ± 50
28.1	153	89	0·60	19·6	0·19	0·1494 ± 0·0048	1·501 ± 0·074	0·0731 ± 0·0027	898 ± 27	1016 ± 76
29.1	511	265	0·53	87·6	0·43	0·1986 ± 0·0070	1·915 ± 0·080	0·0700 ± 0·0017	1168 ± 38	927 ± 49
30.1	386	274	0·73	54·6	0·23	0·1644 ± 0·0043	1·637 ± 0·056	0·0722 ± 0·0015	981 ± 24	993 ± 44
33.1	290	101	0·36	45·6	0·00	0·1830 ± 0·0077	1·894 ± 0·102	0·0751 ± 0·0026	1087 ± 42	1070 ± 68
38.1	459	263	0·59	59·5	0·16	0·1504 ± 0·0041	1·498 ± 0·048	0·0722 ± 0·0013	903 ± 22	992 ± 37
Patchy core										
2.1	891	260	0·30	80·6	0·10	0·1052 ± 0·0027	0·920 ± 0·033	0·0634 ± 0·0016	645 ± 16	723 ± 54
9.1	998	348	0·36	121	0·39	0·1406 ± 0·0038	1·336 ± 0·048	0·0689 ± 0·0016	848 ± 22	896 ± 47
Strongly luminescent rim										
2.2	173	24	0·14	15·7	0·86	0·1049 ± 0·0061	0·983 ± 0·108	0·0680 ± 0·0060	643 ± 35	867 ± 180
3.1	63	16	0·27	8·30	1·50	0·1512 ± 0·0056	1·291 ± 0·155	0·0619 ± 0·0074	908 ± 32	671 ± 250
4.1	103	52	0·52	10·2	1·74	0·1134 ± 0·0086	0·886 ± 0·142	0·0567 ± 0·0085	692 ± 50	478 ± 320
7.1	147	12	0·08	11·8	0·76	0·0928 ± 0·0033	0·772 ± 0·071	0·0604 ± 0·0051	572 ± 20	617 ± 180
9.2	65	18	0·28	6·56	1·66	0·1163 ± 0·0044	0·980 ± 0·147	0·0611 ± 0·0086	710 ± 25	643 ± 310
10.1	96	27	0·29	6·76	0·79	0·0812 ± 0·0029	0·708 ± 0·071	0·0633 ± 0·0060	503 ± 17	718 ± 200
22.1	157	21	0·14	21·0	0·56	0·1550 ± 0·0048	1·369 ± 0·136	0·0640 ± 0·0060	929 ± 27	742 ± 200
23.1	163	29	0·18	11·7	0·26	0·0831 ± 0·0024	0·687 ± 0·036	0·0600 ± 0·0026	514 ± 14	604 ± 95
24.1	116	15	0·13	13·0	0·48	0·1300 ± 0·0038	1·307 ± 0·071	0·0729 ± 0·0033	788 ± 22	1012 ± 91
34.1	102	9	0·09	12·6	0·75	0·1431 ± 0·0043	1·427 ± 0·081	0·0720 ± 0·0035	862 ± 24	987 ± 99
35.1	60	12	0·21	7·12	2·17	0·1354 ± 0·0046	1·072 ± 0·203	0·0574 ± 0·0103	819 ± 26	507 ± 400
36.1	88	24	0·28	9·47	1·07	0·1243 ± 0·0077	1·206 ± 0·107	0·0704 ± 0·0045	755 ± 45	939 ± 130
37.1	121	31	0·27	14·3	0·87	0·1361 ± 0·0050	1·200 ± 0·072	0·0639 ± 0·0030	822 ± 29	739 ± 100
39.1	146	22	0·16	10·5	0·43	0·0831 ± 0·0025	0·685 ± 0·047	0·0598 ± 0·0036	515 ± 15	596 ± 130
Weakly luminescent rim or individual grain										
1.3	319	175	0·57	23·7	0·87	0·0854 ± 0·0024	0·644 ± 0·044	0·0547 ± 0·0034	528 ± 14	401 ± 140
5.1	742	562	0·78	52·1	0·24	0·0815 ± 0·0021	0·656 ± 0·026	0·0584 ± 0·0018	505 ± 13	545 ± 67
12.1	791	564	0·74	61·3	0·24	0·0900 ± 0·0023	0·679 ± 0·024	0·0547 ± 0·0012	556 ± 14	399 ± 50
13.1	650	502	0·80	48·5	0·32	0·0867 ± 0·0024	0·689 ± 0·032	0·0576 ± 0·0022	536 ± 14	516 ± 83
14.1	479	300	0·65	33·4	0·61	0·0806 ± 0·0023	0·628 ± 0·039	0·0565 ± 0·0031	500 ± 14	473 ± 120
16.1	737	504	0·71	56·0	0·18	0·0882 ± 0·0023	0·708 ± 0·025	0·0582 ± 0·0013	545 ± 14	538 ± 50
17.1	528	392	0·77	40·3	0·13	0·0887 ± 0·0024	0·728 ± 0·026	0·0596 ± 0·0014	548 ± 14	588 ± 52
18.1	469	288	0·63	33·8	0·74	0·0832 ± 0·0023	0·641 ± 0·030	0·0559 ± 0·0021	515 ± 14	449 ± 85
19.1	544	353	0·67	41·0	0·20	0·0876 ± 0·0024	0·731 ± 0·028	0·0605 ± 0·0016	541 ± 14	623 ± 57

(continued)

Table 4: Continued

Spot	U(ppm)	Th (ppm)	Th/U	Pb* (ppm)	Common ^{206}Pb (%)	Isotopic ratios			Ages (Ma)	
						$^{206}Pb/^{238}U$	$^{207}Pb/^{235}U$	$^{207}Pb/^{206}Pb$	$^{206}Pb/^{238}U$	$^{207}Pb/^{206}Pb$
31.1	701	509	0·75	54·8	0·22	0·0909 ± 0·0024	0·676 ± 0·028	0·0539 ± 0·0017	561 ± 14	368 ± 71
32.1	680	502	0·76	51·3	0·26	0·0875 ± 0·0023	0·684 ± 0·023	0·0567 ± 0·0012	541 ± 13	478 ± 47
40.1	773	531	0·71	57·5	0·10	0·0866 ± 0·0023	0·723 ± 0·023	0·0605 ± 0·0011	535 ± 13	623 ± 41
41.1	1123	759	0·70	83·7	0·00	0·0867 ± 0·0025	0·694 ± 0·023	0·0581 ± 0·0009	536 ± 15	533 ± 33
42.1	713	633	0·92	52·8	0·22	0·0859 ± 0·0022	0·681 ± 0·023	0·0574 ± 0·0013	531 ± 13	509 ± 48
43.1	537	332	0·64	39·6	0·28	0·0855 ± 0·0023	0·671 ± 0·025	0·0570 ± 0·0015	529 ± 13	490 ± 56
Sample 72-1 (garnet-free mafic granulite)										
Banded grain										
1.1	262	250	0·99	43·9	0·08	0·1949 ± 0·0053	2·112 ± 0·072	0·0786 ± 0·0016	1148 ± 29	1162 ± 40
1.2	527	714	1·40	97·4	0·00	0·2152 ± 0·0056	2·364 ± 0·069	0·0797 ± 0·0010	1256 ± 30	1189 ± 26
2.1	219	182	0·86	29·5	0·22	0·1563 ± 0·0044	1·660 ± 0·060	0·0771 ± 0·0018	936 ± 24	1123 ± 45
3.1	702	890	1·31	79·4	0·04	0·1316 ± 0·0034	1·265 ± 0·038	0·0697 ± 0·0010	797 ± 20	920 ± 31
4.1	1004	1688	1·74	82·1	0·07	0·0951 ± 0·0025	0·808 ± 0·027	0·0616 ± 0·0012	586 ± 15	660 ± 43
5.1	370	387	1·08	53·8	0·14	0·1691 ± 0·0046	1·706 ± 0·055	0·0732 ± 0·0013	1007 ± 25	1018 ± 37
6.1	544	598	1·14	58·8	0·06	0·1257 ± 0·0033	1·169 ± 0·037	0·0675 ± 0·0012	763 ± 19	852 ± 37
7.1	491	539	1·13	75·3	0·04	0·1783 ± 0·0046	1·919 ± 0·058	0·0780 ± 0·0012	1058 ± 26	1148 ± 29
7.2	654	775	1·22	107	0·03	0·1911 ± 0·0052	2·005 ± 0·058	0·0761 ± 0·0009	1127 ± 28	1098 ± 24
8.1	345	317	0·95	41·7	0·09	0·1408 ± 0·0038	1·435 ± 0·049	0·0739 ± 0·0016	849 ± 22	1040 ± 42
9.1	1537	2807	1·89	140	0·03	0·1060 ± 0·0028	0·971 ± 0·027	0·0665 ± 0·0008	649 ± 16	822 ± 24
10.1	1559	2408	1·60	245	0·02	0·1829 ± 0·0046	1·938 ± 0·054	0·0768 ± 0·0009	1083 ± 25	1117 ± 25
11.1	1262	851	0·70	179	0·03	0·1649 ± 0·0043	1·659 ± 0·046	0·0730 ± 0·0009	984 ± 23	1014 ± 24
12.1	5595	2204	0·41	744	0·01	0·1549 ± 0·0043	1·530 ± 0·043	0·0716 ± 0·0003	928 ± 24	976 ± 9
14.1	487	327	0·69	77·7	0·00	0·1858 ± 0·0052	1·930 ± 0·071	0·0753 ± 0·0019	1099 ± 28	1077 ± 50
15.1	1260	1868	1·53	131	0·00	0·1208 ± 0·0031	1·114 ± 0·035	0·0669 ± 0·0011	735 ± 18	835 ± 35
16.1	1070	1621	1·56	122	0·06	0·1327 ± 0·0035	1·280 ± 0·036	0·0699 ± 0·0008	803 ± 19	927 ± 25
17.1	1260	1014	0·83	218	0·03	0·2013 ± 0·0072	2·117 ± 0·078	0·0763 ± 0·0007	1182 ± 39	1102 ± 18
18.1	247	198	0·83	25·5	0·15	0·1202 ± 0·0034	1·128 ± 0·045	0·0681 ± 0·0020	732 ± 19	870 ± 61
19.1	364	213	0·61	44·1	0·33	0·1405 ± 0·0038	1·342 ± 0·050	0·0693 ± 0·0018	847 ± 21	907 ± 53
20.1	1183	1871	1·63	133	0·07	0·1308 ± 0·0037	1·228 ± 0·041	0·0681 ± 0·0012	793 ± 21	871 ± 37
21.1	977	1054	1·11	147	0·05	0·1746 ± 0·0045	1·817 ± 0·051	0·0755 ± 0·0008	1037 ± 25	1081 ± 22
21.2	247	171	0·71	42·0	0·00	0·1980 ± 0·0053	2·205 ± 0·075	0·0808 ± 0·0015	1165 ± 29	1216 ± 38
Moderately luminescent rim										
13.1	296	154	0·54	32·5	0·00	0·1278 ± 0·0041	1·253 ± 0·049	0·0711 ± 0·0016	775 ± 23	960 ± 47
13.2	316	171	0·56	39·0	0·17	0·1435 ± 0·0040	1·406 ± 0·051	0·0710 ± 0·0016	865 ± 22	958 ± 47
Sample 71-7 (paragneiss)										
Weakly luminescent core										
1.1	2756	67	0·02	214	0·01	0·0904 ± 0·0018	0·725 ± 0·016	0·0582 ± 0·0005	558 ± 11	536 ± 17
2.1	2302	632	0·28	330	0·03	0·1669 ± 0·0033	1·750 ± 0·037	0·0761 ± 0·0004	995 ± 19	1096 ± 11
3.1	2596	88	0·04	204	0·04	0·0913 ± 0·0020	0·731 ± 0·017	0·0581 ± 0·0005	563 ± 12	533 ± 18
4.1	1626	102	0·06	134	0·17	0·0957 ± 0·0020	0·765 ± 0·018	0·0580 ± 0·0007	589 ± 12	529 ± 27
5.1	1774	172	0·10	245	0·08	0·1605 ± 0·0034	1·540 ± 0·035	0·0696 ± 0·0007	959 ± 18	916 ± 19
6.1	2115	67	0·03	170	0·08	0·0936 ± 0·0019	0·748 ± 0·017	0·0580 ± 0·0006	577 ± 11	528 ± 21
7.1	844	53	0·07	66·8	0·11	0·0921 ± 0·0021	0·709 ± 0·020	0·0558 ± 0·0008	568 ± 13	445 ± 33
8.1	2187	136	0·06	295	0·12	0·1570 ± 0·0031	1·518 ± 0·033	0·0701 ± 0·0005	940 ± 18	932 ± 15
9.1	1294	77	0·06	96·1	0·09	0·0864 ± 0·0018	0·680 ± 0·018	0·0571 ± 0·0009	534 ± 11	496 ± 33

Table 4: Continued

Spot	U(ppm)	Th (ppm)	Th/U	Pb* (ppm)	Common ^{206}Pb (%)	Isotopic ratios			Ages (Ma)	
						^{206}Pb/^{238}U	^{207}Pb/^{235}U	^{207}Pb/^{206}Pb	^{206}Pb/^{238}U	^{207}Pb/^{206}Pb
Moderately luminescent rim										
1.2	740	117	0·16	57·4	0·17	0·0902 ± 0·0022	0·700 ± 0·021	0·0563 ± 0·0010	556 ± 13	465 ± 38
6.2	172	177	1·06	12·9	0·53	0·0867 ± 0·0021	0·702 ± 0·048	0·0587 ± 0·0038	536 ± 12	556 ± 140
10.1	452	211	0·48	32·2	0·20	0·0828 ± 0·0018	0·656 ± 0·021	0·0574 ± 0·0013	513 ± 11	508 ± 51
11.1	225	289	1·33	17·0	1·49	0·0867 ± 0·0020	0·660 ± 0·052	0·0552 ± 0·0041	536 ± 12	420 ± 170
12.1	293	136	0·48	21·8	0·90	0·0858 ± 0·0020	0·670 ± 0·040	0·0566 ± 0·0031	531 ± 12	477 ± 120
13.1	169	91	0·56	12·6	0·74	0·0863 ± 0·0021	0·677 ± 0·036	0·0569 ± 0·0028	534 ± 12	189 ± 110
14.1	209	187	0·92	16·2	0·92	0·0891 ± 0·0021	0·748 ± 0·052	0·0609 ± 0·0039	550 ± 13	634 ± 140
15.1	231	89	0·40	17·3	1·02	0·0865 ± 0·0021	0·704 ± 0·052	0·0591 ± 0·0041	535 ± 12	569 ± 150
16.1	214	250	1·21	16·5	0·56	0·0894 ± 0·0021	0·691 ± 0·040	0·0561 ± 0·0030	552 ± 13	456 ± 120
16.2	251	121	0·50	17·8	0·72	0·0819 ± 0·0021	0·635 ± 0·045	0·0562 ± 0·0037	508 ± 13	462 ± 150
17.1	168	208	1·28	12·9	0·93	0·0883 ± 0·0037	0·667 ± 0·067	0·0548 ± 0·0050	545 ± 22	403 ± 210
18.1	235	115	0·51	17·0	0·24	0·0840 ± 0·0020	0·693 ± 0·028	0·0598 ± 0·0019	520 ± 12	597 ± 69
Sample 72-7 (orthogneiss)										
Oscillatory-zoned core										
1.1	808	760	0·97	124	0·04	0·1789 ± 0·0038	1·966 ± 0·045	0·0797 ± 0·0007	1061 ± 21	1189 ± 18
2.1	927	603	0·67	137	0·08	0·1724 ± 0·0036	1·793 ± 0·041	0·0754 ± 0·0007	1025 ± 20	1080 ± 19
3.1	368	238	0·67	55·7	0·17	0·1761 ± 0·0042	1·838 ± 0·051	0·0757 ± 0·0011	1046 ± 24	1087 ± 28
4.1	620	383	0·64	72·7	0·19	0·1364 ± 0·0029	1·366 ± 0·041	0·0727 ± 0·0016	824 ± 16	1005 ± 44
5.1	275	130	0·49	45·3	0·15	0·1914 ± 0·0042	2·107 ± 0·059	0·0798 ± 0·0014	1130 ± 22	1192 ± 35
5.2	397	80	0·21	62·4	0·13	0·1825 ± 0·0038	1·983 ± 0·050	0·0788 ± 0·0010	1081 ± 21	1168 ± 27
7.1	320	141	0·45	56·7	0·00	0·2061 ± 0·0045	2·313 ± 0·058	0·0814 ± 0·0011	1208 ± 24	1232 ± 25
8.1	542	293	0·56	94·1	0·09	0·2019 ± 0·0042	2·152 ± 0·049	0·0773 ± 0·0008	1186 ± 23	1129 ± 21
9.1	359	186	0·54	59·8	0·16	0·1937 ± 0·0043	2·062 ± 0·052	0·0772 ± 0·0010	1141 ± 23	1127 ± 26
10.1	447	246	0·57	76·5	0·06	0·1993 ± 0·0041	2·161 ± 0·052	0·0787 ± 0·0009	1171 ± 23	1164 ± 24
11.1	478	311	0·67	68·4	0·12	0·1665 ± 0·0037	1·694 ± 0·042	0·0738 ± 0·0010	993 ± 20	1036 ± 27
12.1	314	161	0·53	54·7	0·19	0·2023 ± 0·0045	2·314 ± 0·062	0·0729 ± 0·0012	1188 ± 24	1268 ± 28
13.1	354	217	0·63	49·4	0·12	0·1625 ± 0·0034	1·730 ± 0·043	0·0772 ± 0·0009	971 ± 19	1126 ± 25
14.1	275	247	0·93	48·0	0·26	0·2030 ± 0·0045	2·200 ± 0·062	0·0786 ± 0·0014	1191 ± 24	1162 ± 35
15.1	473	227	0·50	79·1	0·03	0·1948 ± 0·0043	2·136 ± 0·053	0·0795 ± 0·0010	1147 ± 23	1185 ± 23
16.1	554	257	0·48	85·3	0·11	0·1788 ± 0·0038	1·832 ± 0·044	0·0743 ± 0·0010	1061 ± 21	1050 ± 25
17.1	636	375	0·61	119	0·11	0·2169 ± 0·0046	2·366 ± 0·059	0·0791 ± 0·0010	1265 ± 24	1175 ± 26
Moderately luminescent rim										
4.2	77	185	2·49	5·70	0·83	0·0859 ± 0·0023	0·706 ± 0·063	0·0597 ± 0·0051	531 ± 14	591 ± 180
6.1	86	316	3·80	6·55	4·34	0·0848 ± 0·0025	0·407 ± 0·147	0·0348 ± 0·0125	524 ± 15	
10.2	181	277	1·58	13·5	0·34	0·0864 ± 0·0020	0·705 ± 0·048	0·0592 ± 0·0038	534 ± 12	573 ± 140
13.2	68	210	3·19	4·98	1·19	0·0842 ± 0·0024	0·702 ± 0·062	0·0605 ± 0·0051	521 ± 14	620 ± 180
14.2	98	254	2·68	7·34	0·71	0·0867 ± 0·0023	0·734 ± 0·050	0·0613 ± 0·0038	536 ± 14	651 ± 130
15.2	92	295	3·30	6·84	1·65	0·0847 ± 0·0023	0·608 ± 0·079	0·0520 ± 0·0062	524 ± 14	287 ± 280

Pb* denotes radiogenic Pb. Common ^{206}Pb (%) represents the proportion of common ^{206}Pb in total ^{206}Pb measured. Common Pb was corrected using the measured ^{204}Pb and a model common Pb composition (Stacey & Kramers, 1975) appropriate to the age of the mineral. All uncertainties are 1σ.

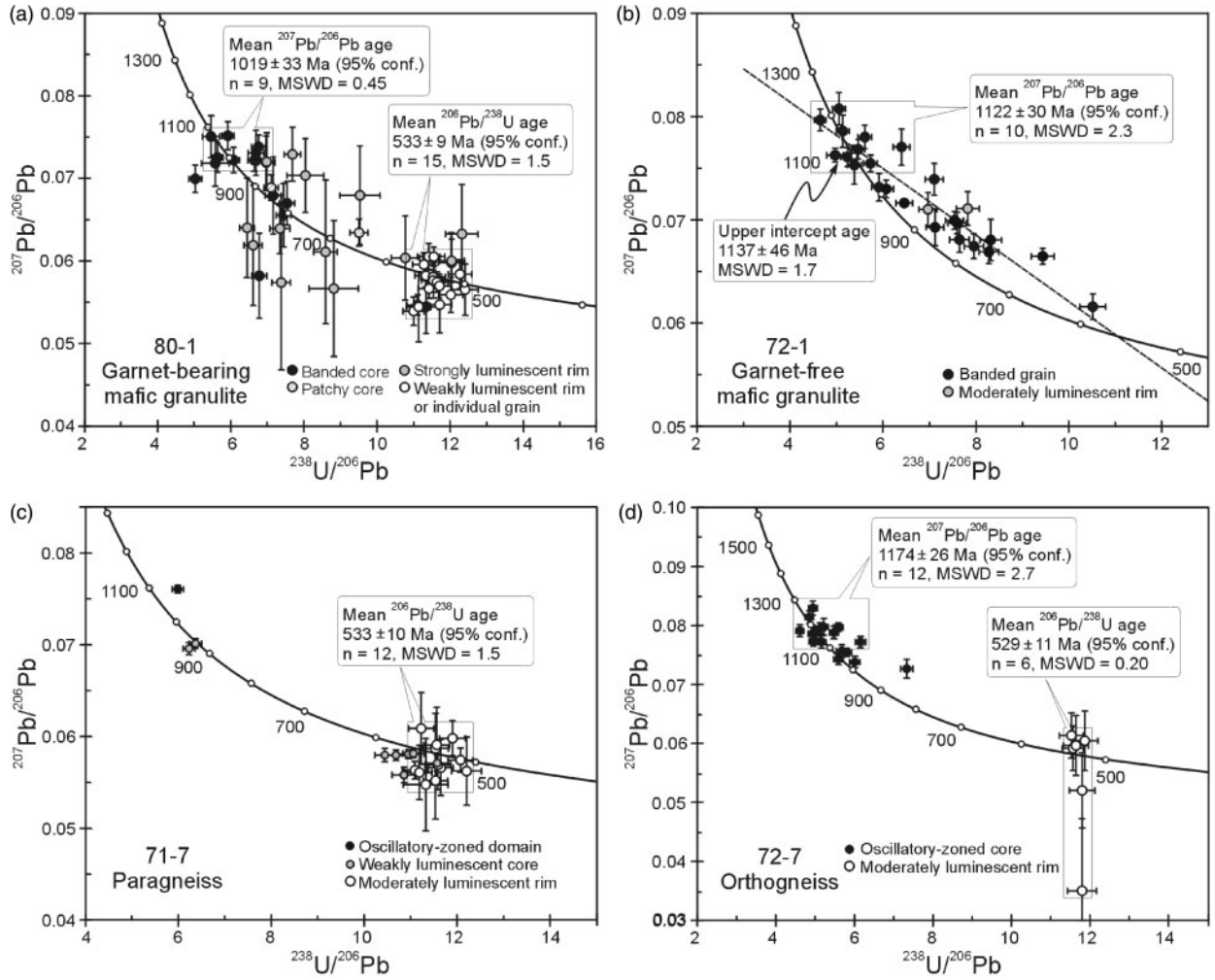

Fig. 10. Tera–Wasserburg (TW) concordia diagrams for zircons from granulites in the McKaskle Hills. (a) Garnet-bearing mafic granulite (sample 80-1). (b) Garnet-free mafic granulite (sample 72-1). (c) Paragneiss (sample 71-7). (d) Orthogneiss (sample 72-7).

obtained for these zircon domains probably reflect partial or entire resetting of the U–Pb isotopic system during Cambrian recrystallization of pre-existing zircons. They are consequently inferred to provide no meaningful geological data. Alternatively, these ages could represent a late Mesoproterozoic–early Neoproterozoic thermal event at ~1000 Ma that has been strongly reworked by a later Cambrian metamorphic event at ~530 Ma. However, inferring a metamorphic event without new zircon growth and/or age clustering seems unlikely. Importantly, weakly luminescent rims have never been observed to grow on strongly luminescent domains, suggesting that these two zircon domains were not formed by two separate metamorphic events. Moreover, the presence of Cambrian metamorphic zircons growing directly on the Mesoproterozoic magmatic zircon domains in orthogneiss sample 72-7 (see below) does not support the occurrence of a ~1000 Ma thermal event in the area.

Sample 72-1: garnet-free mafic granulite

Garnet-free mafic granulite sample 72-1 is representative of the regional two-pyroxene mafic granulites in the McKaskle Hills. Zircons from this rock are also colorless or pale yellow and rounded to prismatic in shape. They have grain lengths of 50–180 μm. All zircon grains have moderate to weak CL response and preserve banded zoning (Fig. 9g and h). Similar to sample 80-1, this zoning is interpreted to reflect a magmatic origin that may have been affected by solid-state recrystallization. Amphibole, clinopyroxene, plagioclase, quartz and apatite were found as inclusions in these zircons. The bands in the weakly luminescent grains are commonly thickened. Some such grains are partially embayed by moderately luminescent rims (Fig. 9h and i), which are interpreted to have formed during recrystallization of igneous zircon. Local, weakly luminescent overgrowths also occur on some zircon grains (Fig. 9h). These are assumed to be the expression of

Cambrian metamorphic growth, but the domains are too thin to be analyzed.

Twenty-five analyses on 21 zircon grains were performed on this sample (Table 4 and Fig. 10b). The banded zircons show a scattered age distribution ranging from 1216 ± 38 Ma ($^{207}Pb/^{206}Pb$ age) to 586 ± 15 Ma ($^{206}Pb/^{238}U$ age), with Th/U ratios ranging from 0·69 to 1·74. However, 10 analyses ($^{207}Pb/^{206}Pb$ ages ranging from 1216 ± 38 Ma to 1077 ± 50 Ma) form a nearly concordant cluster giving a weighted mean $^{207}Pb/^{206}Pb$ age of 1122 ± 30 Ma (MSWD = 2·3). The remaining 13 analyses show different degrees of discordance produced by radiogenic Pb loss. Two ages from moderately luminescent rims are also discordant and show appreciable Pb loss. When combined, all 25 datasets yield a discordia with an upper intercept age of 1137 ± 46 Ma and a lower intercept age of 560 ± 58 Ma (MSWD = 1·7). The upper intercept age is equivalent within error to the mean age obtained from the banded zircon domains and is interpreted as the minimum emplacement age of the mafic granulite protolith. The inaccurate lower intercept age could reflect the effect of a metamorphic event at ~530 Ma as revealed by sample 80-1.

Sample 71-7: paragneiss

Zircons from paragneiss sample 71-7 are pale yellow and rounded in shape and have grain sizes ranging from 30 to 100 μm. Both optical and CL images reveal a typical core–rim structure (Fig. 9j–n) for almost all the zircon grains. All the cores are small and well-rounded. Therefore, they are interpreted to be of detrital origin. These cores have extremely low CL response and appear unstructured or sector-zoned. In addition, an oscillatory-zoned domain is preserved in the inner part of a such core (Fig. 9j), which may represent a relic of an earlier igneous zircon. All the rims grew around a detrital core and show moderate CL response and planar growth banding or fir-tree sector zoning. Some grains have a weakly luminescent mantle and a moderately luminescent rim (Fig. 9k). Radial fractures developed around a detrital core are commonly visible in transmitted light (Fig. 9n). These rims are interpreted to be of metamorphic origin.

Twenty-one U–Pb analyses on 18 zircon grains reveal three age populations (Table 4 and Fig. 10c). The oldest $^{207}Pb/^{206}Pb$ age of 1096 ± 11 Ma (spot 2.1) was obtained for an oscillatory-zoned domain within a weakly luminescent core, with a Th/U ratio of 0·28. Two other weakly luminescent cores yield $^{207}Pb/^{206}Pb$ ages of 932 ± 15 Ma (spot 8.1) and 916 ± 19 Ma (spot 5.1). Their Th/U ratios are very low (<0·10), typical of metamorphic zircon (e.g. Williams & Claesson, 1987; Rubatto & Gebauer, 2000). It should be noted that these two analyses are probably mixed with some rim composition because of the small size of the cores. However, because of the low U concentrations of the rim, the effect of this mixture will be minimal. The remaining six weakly luminescent cores show younger $^{207}Pb/^{206}Pb$ ages between 536 ± 17 Ma and 445 ± 33 Ma. These grains have Th/U ratios of 0·02–0·07 and show reverse discordance, which is interpreted to be due to high uranium contents (Williams, 1998). The $^{206}Pb/^{238}U$ ages obtained from the moderately luminescent rims give ages between 556 ± 13 Ma and 508 ± 13 Ma, with a mean of 533 ± 10 Ma (n = 12, MSWD = 1·5). Th/U ratios for these domains range from 0·16 to 1·33. The ages of zircon rims are interpreted to represent the timing of metamorphism of the paragneiss. In contrast, two concordant data for detrital zircon cores are interpreted as the minimum age of early Neoproterozoic metamorphism, whereas other detrital zircon cores may have experienced recrystallization during the Cambrian metamorphism. The age of the oscillatory-zoned zircon domains is in agreement with the ages of igneous events obtained from other samples.

Sample 72-7: orthogneiss

Zircons from orthogneiss sample 72-7 are pale brown and prismatic, and 200–380 μm in length. They all show simple zoning patterns characterized by oscillatory-zoned cores and moderately luminescent overgrowths (Fig. 9o and p). Biotite, K-feldspar, plagioclase, quartz, magnetite and apatite were observed as inclusions in the oscillatory-zoned cores. The overgrowths show planar growth banding and sector zoning and are interpreted to have formed during metamorphism.

The results of 23 analyses on 17 zircon grains form two populations (Table 4 and Fig. 10d). Oscillatory-zoned cores give $^{207}Pb/^{206}Pb$ ages ranging from 1268 ± 28 Ma to 1005 ± 44 Ma, with Th/U ratios ranging from 0·21 to 0·97. Of these, 12 concordant analyses yield a weighted mean age of 1174 ± 26 Ma (MSWD = 2·7). This age is interpreted as the igneous emplacement age of the orthogneiss protolith. The other five analyses showing younger ages probably reflect Pb loss caused by the subsequent metamorphism. The $^{206}Pb/^{238}U$ ages obtained for six moderately luminescent overgrowths form a single population (536 ± 14 Ma to 521 ± 14 Ma) with a mean of 529 ± 11 Ma (MSWD = 0·20). These overgrowths have low U but high Th concentrations with high Th/U ratios of 1·58–3·80. The age is interpreted to represent the timing of metamorphic recrystallization of the orthogneiss.

Sm–Nd mineral-whole-rock dating

The coarse-grained garnet, clinopyroxene and orthopyroxene in the mafic granulites and garnet, orthopyroxene, biotite and plagioclase in the paragneisses were separated for Sm–Nd isotopic dating. In the mafic granulites, symplectic clinopyroxene and orthopyroxene are easily separated because of their fine-grained size and intergrowth with plagioclase, whereas amphibole and plagioclase were not selected for isotopic analyses because of their multiple

Table 5: Sm–Nd isotopic compositions of mafic granulites and paragneisses from the McKaskle Hills

Whole-rock and mineral	Sm (ppm)	Nd (ppm)	$^{147}Sm/^{144}Nd$	$^{143}Nd/^{144}Nd$	±2σm	Isochron age (Ma)	Initial ratio (metamorphic)	$\varepsilon Nd(T)$	T_{DM^1} (Ga)	T_{DM^2} (Ga)
Sample 70-11 (mafic granulite)										
WR	3·755	12·07	0·1880	0·512380	13	500 ± 9	0·511763 ± 22	−3·9	4510	1950
Grt	3·777	2·556	0·8934	0·514692	12					
Cpx	6·380	22·33	0·1727	0·512332	12					
Opx	0·4395	1·264	0·2102	0·512449	13					
Sample 80-1 (mafic granulite)										
WR	8·090	44·95	0·1088	0·511846	13	499 ± 10*	0·511481 ± 23	−4·0	1890	1970
Grt	5·196	4·543	0·6913	0·513740	13					
Cpx	8·248	38·46	0·1297	0·511956	14					
Opx	0·6785	3·030	0·1354	0·511914	12					
Sample 71-7 (paragneiss)										
WR	3·852	15·92	0·1463	0·511967	13	495 ± 6	0·511491 ± 15	−9·9	2660	2020
Grt	14·51	5·464	1·6051	0·516701	13					
Opx	0·8865	1·962	0·2731	0·512356	13					
Bt	0·7840	3·777	0·1255	0·511908	12					
Pl	3·258	19·59	0·1006	0·511819	10					
Sample 70-6 (paragneiss)										
WR	7·297	31·13	0·1417	0·512113	14	457 ± 12†	0·511586 ± 25	−7·0	2190	1760
Grt	13·52	14·58	0·5609	0·513262	13					
Opx	1·413	4·624	0·1848	0·512147	12					
Pl	3·248	21·54	0·0912	0·511852	10					

*Excluding Cpx. †Excluding WR.
Mineral abbreviations are after Kretz (1983), except for whole rock (WR).

growths. However, garnet crystals commonly contain small amounts of mineral inclusions, of which REE-rich minerals, such as apatite and zircon, could be responsible for the increase of Sm and Nd concentrations and possible modification of Sm/Nd ratios in garnet. However, because the peak metamorphic temperatures are higher than the Nd isotope closure temperatures of the inclusions, the Nd isotopic compositions of the inclusions would be expected to attain isotopic equilibrium with the host garnet. Consequently, an isochron constructed with such garnet and cogenetic phases can still provide a correct age of metamorphism (Jahn *et al.*, 2005).

Sm–Nd isotope data for four samples are presented in Table 5 and further illustrated in Fig. 11. Minerals and whole-rock isochron ages from two mafic granulites and one paragneiss are nearly identical, 500 ± 9 Ma (MSWD = 0·04) for sample 70-11, 499 ± 10 Ma (MSWD = 1·06) for sample 80-1, and 495 ± 6 Ma (MSWD = 0·97) for sample 71-7. The initial $^{143}Nd/^{144}Nd$ ratios (I_{Nd}) are 0·511763 ± 0·000022, 0·511481 ± 0·000023 and 0·511491 ± 0·000015, respectively. The data for clinopyroxene from sample 80-1 deviated significantly from the garnet–orthopyroxene–whole-rock trend line and therefore were not involved in the age calculations. The Sm–Nd system for this clinopyroxene seems to have been disturbed during retrogression. The age results of 500–495 Ma are similar to those (515–490 Ma) obtained from granulites in Prydz Bay (Hensen & Zhou, 1995). The whole-rock Sm–Nd results for paragneiss sample 70-6 show a significant deviation from the garnet–orthopyroxene–plagioclase mineral isochron. In addition, the mineral isochron gives a slightly younger age of 457 ± 12 Ma with MSWD = 0·66 and $I_{Nd} = 0·511586 ± 0·000025$. This suggests that the minerals may have re-equilibrated at a later time, or, more likely, isotopic disequilibrium between minerals yields an erroneous isochron. Similarly young ages were also reported from Bolingen Islands, Prydz Bay (Hensen & Zhou, 1995).

The whole-rock analyses for two mafic granulites yield a two-point age of 1027 ± 50 Ma ($I_{Nd} = 0·511113 ± 0·000052$). This age is consistent within error with the U–Pb age obtained for the banded zircon domains from sample 80-1, and therefore supports the interpretation that the protoliths of the mafic granulite were emplaced during

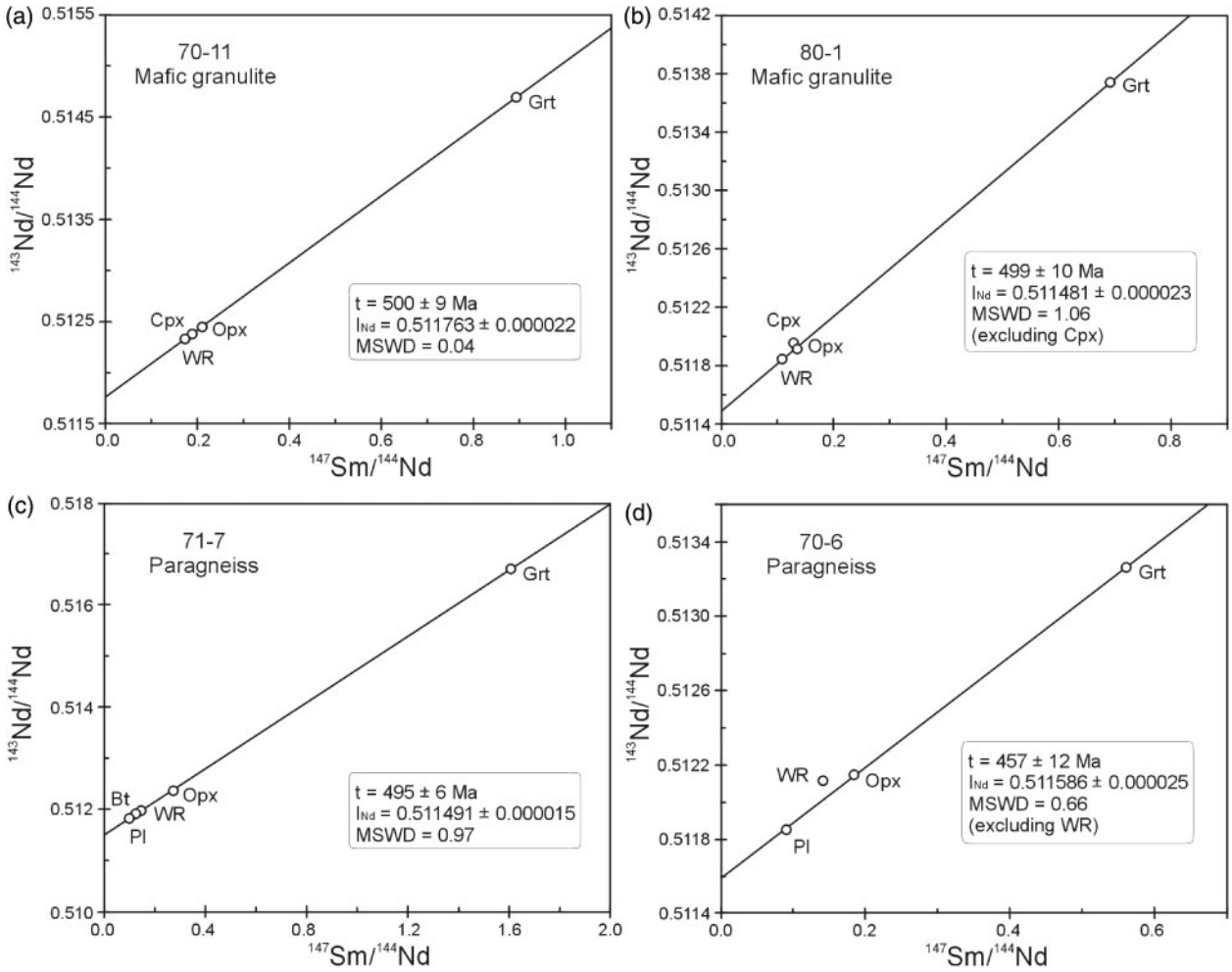

Fig. 11. Sm–Nd mineral–whole-rock isochron diagrams for granulites in the McKaskle Hills. (a) Mafic granulite (sample 70-11). (b) Mafic granulite (sample 80-1). (c) Paragneiss (sample 71-1). (d) Paragneiss (sample 70-6).

late Mesoproterozoic time. Two mafic granulites have $\varepsilon_{Nd}(T)$ values of −3·9 and −4·0, with Nd model ages (T_{DM^1}) of 4510 and 1890 Ma. This could suggest that the primary mafic magma was derived from the partial melting of an enriched subcontinental lithospheric mantle. The old (T_{DM^1}) age obtained for sample 70-11 may be caused by the unreasonably high $^{147}Sm/^{144}Nd$ ratio of the rock. Because two paragneisses have $^{147}Sm/^{144}Nd$ ratios (>0·14) higher than the average crustal ratio of 0·12, it is considered that the two-stage Nd model ages are more realistic for inferring the age of the source. The obtained T_{DM^2} ages for two samples are 2030 and 1780 Ma, respectively.

DISCUSSION

Peak *P–T* conditions and *P–T–t* path of Cambrian metamorphism

Based on geochronological data as well as microstructural and thermobarometric analyses from the Søstrene Island of Prydz Bay, most geologists have accepted that the Prydz Belt is a polymetamorphic belt that was affected by at least two episodes of high-grade metamorphism, in early Neoproterozoic and Cambrian times. The Cambrian metamorphic peak in this belt only reached low- to medium-pressure granulite-facies conditions (6–7 kbar and 760–860°C) (Motoyoshi *et al.*, 1991; Nichols & Berry, 1991; Thost *et al.*, 1994; Fitzsimons, 1996; Carson *et al.*, 1997), whereas the early Neoproterozoic metamorphism took place at relatively high-pressure and high-temperature conditions (9–10 kbar and 850–980°C) (Thost *et al.*, 1991; Hensen *et al.*, 1995; Tong & Liu, 1997). Moreover, in the Rauer Group, two distinct granulite-facies events have been recognized in the metapelites (Harley, 1987; Sims *et al.*, 1994; Dirks & Wilson, 1995; Harley *et al.*, 1998). It seems that Prydz Bay provides an excellent example showing that mineral reaction textures in a granulite sample may not necessarily reflect a single metamorphic cycle with only one *P–T* path. However, based on the

result of *in situ* (Th + U)–Pb monazite dating, Kelsey *et al.* (2003*a*) have argued that the ultrahigh-temperature metamorphism at ~950–1050°C and ~9·5–12 kbar and the subsequent overprint at >800–850°C and >7 kbar as recorded in the metapelites of the Rauer Group (e.g. Harley & Fitzsimons, 1991; Harley, 1998; Kelsey *et al.*, 2003*b*) could have occurred during the same Cambrian event.

Granulites from the McKaskle Hills also preserve two-stage mineral assemblages that recrystallized at 9·0–9·5 kbar and 880–950°C and 6·6–7·2 kbar and 700–750°C, respectively. These P–T estimates seem to be comparable with the P–T conditions of the two metamorphic events in Prydz Bay. However, U–Pb zircon and Sm–Nd mineral–whole-rock data, particularly the growth of new zircon rims on the early Neoproterozoic detrital zircon grains in the paragneiss, clearly suggest that the peak mineral assemblages of granulites from the McKaskle Hills were formed during the Cambrian metamorphism. This implies that the peak P–T conditions of the Cambrian high-grade event in the area are higher than those recorded in much of the Prydz Belt, and the inferred clockwise P–T path for the rocks is related to a single Cambrian metamorphic cycle, rather than two separate metamorphic events. A recent geochronological study of high-grade rocks from the Grove Mountains has revealed that zircon rims with ages of 550–535 Ma grew on magmatic zircon cores with ages of 920–910 Ma (X. Liu *et al.*, 2007), also negating the existence of an early Neoproterozoic metamorphic event in that area. In fact, the recognition of a distinct two-stage decompression in the mafic granulites from Søstrene Island (Thost *et al.*, 1991; Hensen *et al.*, 1995) suggests a different metamorphic evolution compared with other granulites from the Prydz Belt. If so, it is likely that Søstrene Island represents a distinct terrane in the Prydz Belt and that this terrane might have no universal significance. As for the Rauer Group, there is still some possible disagreement in the timing of the ultrahigh-temperature event (Harley, 2003; Hokada *et al.*, 2003; Tong & Wilson, 2006).

There is a difference of ~30 Myr between the ages given by the U–Pb zircon and Sm–Nd mineral–whole-rock dating methods for the granulites from the McKaskle Hills. The closure temperature for the zircon U–Pb system is >900°C (Lee *et al.*, 1997; Cherniak & Watson, 2001) although zircon can grow at very low temperatures (≤550°C) in the presence of hydrous fluids (Rubatto *et al.*, 1999; Liermann *et al.*, 2002). In contrast, the closure temperature for the garnet Sm–Nd system remains controversial, ranging from 850°C for rapidly cooled terranes (Cohen *et al.*, 1988; Jagoutz, 1988) to 600–650°C for slowly cooled ones (Humphries & Cliff, 1982; Mezger *et al.*, 1992; Burton *et al.*, 1995). This suggests that the age difference of ~30 Myr in the present case is likely to result from the difference in closure temperature between the two isotopic systems. Accordingly, the U–Pb zircon age of ~530 Ma is interpreted as the approximate age of the peak metamorphism, whereas the Sm–Nd isochron age of ~500 Ma is interpreted as a decompressional cooling age. The time interval between the peak metamorphism and the blocking of the garnet Sm–Nd isotopic system defines a cooling rate of ~7°C/Ma for granulites from the McKaskle Hills.

Precambrian history and regional correlations

SHRIMP U–Pb zircon dating of mafic granulite and orthogneiss from the McKaskle Hills reveals a mafic–felsic igneous intrusion at ~1170–1020 Ma. These late Mesoproterozoic igneous rocks have been attributed to form part of the basement rocks in Prydz Bay (Fitzsimons & Harley, 1991; Dirks & Hand, 1995; Dirks & Wilson, 1995). The interpretation of the deposition ages of the cover sequence, characterized by migmatitic paragneisses in Prydz Bay, is arguable, with one school of thought considering it to be Mesoproterozoic (Dirks & Wilson, 1995; Carson *et al.*, 1996), whereas others have interpreted it to be Neoproterozoic (Hensen & Zhou, 1995; Zhao *et al.*, 1995). A few zircon domains from paragneiss sample 71-7 collected from the McKaskle Hills record an igneous event at 1096 Ma and a metamorphic event at 932–916 Ma. Such zircon domains are clearly of detrital origin as revealed by optical and CL images. This suggests that at least some paragneiss protoliths in the Prydz Belt were deposited during the Neoproterozoic. As the age of one detrital zircon population from the paragneiss is in good agreement with the ages of granulite facies metamorphism in the Rayner Complex (Young & Black, 1991; Boger *et al.*, 2000; Kelly *et al.*, 2002), it is believed that the materials of the paragneiss sequence came from a similar early Neoproterozoic orogen. The comparable T_{DM} ages between the rocks from two areas lends support to this assumption.

The ages of ~1170–1020 Ma obtained for the mafic granulites and orthogneisses demonstrate that the basement of the McKaskle Hills differs from the Rayner Complex of the nPCM, where all the igneous and metamorphic rocks were dated at <990 Ma except for a leucosome that yielded an inherited age of 1017 Ma (Boger *et al.*, 2000). This suggests that the Rayner Complex does not extend to the east of the Lambert graben and form part of the Prydz Belt. Within East Antarctica, 1170–1040 Ma volcanic and intrusive events have been reported for the rocks in Dronning Maud Land (Harris *et al.*, 1995; Jacobs *et al.*, 1998, 2003; Paulsson & Austrheim, 2003; Board *et al.*, 2005), the Fisher terrane of the nPCM (Beliatsky *et al.*, 1994; Kinny *et al.*, 1997; Mikhalsky *et al.*, 1999) and the Bunger Hills–Windmill Islands area (Sheraton *et al.*, 1990, 1992; Post *et al.*, 1997). Additionally, ~1300 Ma felsic volcanism and intrusion have also been reported for the rocks in the

Fisher terrane. These Mesoproterozoic igneous events occurred in different tectonic settings, including a volcanic arc in Dronning Maud Land, an active continental margin in the Fisher terrene, and a post-orogenic environment in the Bunger Hills–Windmill Islands area. Rocks from the McKaskle Hills might also have formed at an active continental margin as inferred from the orthogneisses of the Jennings Promontory, 25 km SW of the McKaskle Hills (Sheraton *et al.*, 1996); however, their low $\varepsilon_{Nd}(T)$ values are distinct from those of juvenile rocks from the Fisher terrane. Furthermore, the above three areas have all experienced late Mesoproterozoic medium- to high-grade metamorphism, although the metamorphism in the different areas was not contemporaneous. Therefore, the McKaskle Hills (and possibly the entire EAIS) might record a Precambrian history different from that of the Mesoproterozoic–Neoproterozoic terranes in East Antarctica and should represent a distinct basement terrane.

Implications for the evolution of the Prydz Belt

U–Pb zircon ages of 533–529 Ma for regional metamorphism in the McKaskle Hills, together with a U–Th–total Pb monazite age of 536 Ma obtained for a pegmatite in the Reinbolt Hills (Ziemann *et al.*, 2005) and a U–Pb zircon age of 500 Ma obtained for a granite at Landing Bluff (Tingey, 1991), suggest that the EAIS is a part of the Prydz Belt. However, the different units in the Prydz Belt seem to record a different earlier tectonic evolution, although all of them have experienced the same intense Cambrian high-grade metamorphic episode. The Larsemann Hills resemble the McKaskle Hills by preserving an igneous event at ~1100 Ma, but subsequent metamorphism and granite emplacement at 990–940 Ma have also occurred within the basement in this area (Hensen *et al.*, 1995; Zhao *et al.*, 1995; Wang *et al.*, 2003). In the Grove Mountains, a mafic–felsic intrusive event has been dated at 920–910 Ma, and the detrital zircons from a paragneiss preserve an early Paleoproterozoic age of ~2050 Ma (X. Liu *et al.*, 2007). In the Rauer Group and in the northern part of the sPCM, Cambrian high-grade metamorphism was overprinted on the Archaean basement rocks (Kinny *et al.*, 1993; Harley *et al.*, 1998; Boger *et al.*, 2001). The existence of multiple basement terranes in an orogen and the lack of similar terranes outside the orogen is difficult to interpret by an intracontinental reworking model as favored by some workers (e.g. Yoshida, 1995; Wilson *et al.*, 1997; Yoshida *et al.*, 2003).

The shape of the P–T path provides an indication of the tectonic processes involved in the formation and evolution of the granulites (e.g. Harley, 1989). The relatively high peak P–T conditions followed by decompression of 2–3 kbar inferred from the granulites in the McKaskle Hills indicate a considerable crustal thickening subsequently followed by tectonic uplift and unroofing during the Cambrian orogeny. This scenario is consistent with the widespread development of contemporaneous compressional and subsequent extensional deformation in the Prydz Belt (Carson *et al.*, 1995; Dirks & Wilson, 1995; Liu *et al.*, 2006). The intrusion of voluminous syn- to post-orogenic granitoids in the belt, particularly the widespread distribution of intermediate charnockites and sheeted granites in the Grove Mountains, suggests that lithospheric delamination and asthenospheric upwelling could have occurred during post-collisional extension (Liu *et al.*, 2006). Coupled with the juxtaposition of multiple basement terranes, we favor the suggestion that the Prydz Belt represents a collisional orogen that resulted from the assembly of Gondwana during Cambrian times (e.g. Fitzsimons, 2000, 2003; Boger *et al.*, 2001; Zhao *et al.*, 2003).

CONCLUSIONS

U–Pb zircon and Sm–Nd mineral–whole-rock dating of mafic granulites and felsic gneisses from the McKaskle Hills reveals a peak metamorphic age of 533–529 Ma and a cooling age of ~500 Ma, respectively. Hence the area is attributed to a part of the Prydz Belt. Thermobarometric estimates from mafic granulites suggest that the Cambrian metamorphism reached peak pressures of 9·0–9·5 kbar at 880–950°C during crustal thickening, followed by decompression to 6·6–7·2 kbar at 700–750°C as a consequence of orogenic exhumation and unroofing. U–Pb zircon dating also reveals that the basement of mafic granulites and orthogneisses in the McKaskle Hills was formed during a time interval of 1170–1020 Ma, whereas the cover sequence (now paragneisses) was deposited on the basement during the Neoproterozoic. This basement is not only distinct from the nPCM by its old protolith crystallization ages, but also slightly different from that of Prydz Bay by the absence of an early Neoproterozoic metamorphic event. Taking into account multiple basement juxtaposition and a clockwise P–T–t path, we prefer the suggestion that the Prydz Belt represents a collisional orogen that resulted from the assembly of Gondwana during the Cambrian period.

ACKNOWLEDGEMENTS

We would like to thank Liudong Ren for assistance during field work and for fruitful discussions and valuable comments on the manuscript. Zhuyin Chu and Ji Qiu ably assisted in the Sm–Nd isotopic analyses, and Guiming Shu in the electron microprobe analyses. N. M. Kelly, S. D. Boger, D. E. Kelsey, M. J. Flowerdew and R. W. White are thanked for their detailed and thorough critical reviews, and G. L. Clarke for his editorial comments, which not only greatly improved the manuscript, but also

improved the English expression. The field work was carried out during the 2004–2005 Chinese National Antarctic Research Expedition. Logistic support by the Antarctic Administration of China and financial support by the Geological Investigation Project of the Chinese Geological Survey (1212010511505), National Natural Science Foundation of China (No. 40372046) and Programme of Young Scientists of the Ministry of Land and Resources are gratefully acknowledged.

SUPPLEMENTARY DATA

Supplementary data for total microprobe analyses of minerals in this paper are available at *Journal of Petrology* online.

REFERENCES

Aranovich, L. Y. & Berman, R. G. (1997). A new garnet–orthopyroxene thermometer based on reversed Al_2O_3 solubility in FeO–Al_2O_3–SiO_2 orthopyroxene. *American Mineralogist* **82**, 345–353.

Bégin, N. J. & Pattison, D. R. M. (1994). Metamorphic evolution of granulites in the Minto Block, northern Québec: extraction of peak P–T conditions taking account of late Fe–Mg exchange. *Journal of Metemorphic Geology* **12**, 411–428.

Beliatsky, B. V., Laiba, A. A. & Mikhalsky, E. V. (1994). U–Pb zircon age of the metavolcanic rocks of Fisher Massif (Prince Charles Mountains, East Antarctica). *Antarctic Science* **6**, 355–358.

Berman, R. G. & Aranovich, L. Y. (1996). Optimized standard state and mixing properties of minerals: I. Model calibration for olivine, orthopyroxene, cordierite, garnet and ilmenite in the system FeO–MgO–CaO–Al_2O_3–SiO_2–TiO_2. *Contributions to Mineralogy and Petrology* **126**, 1–24.

Black, L. P., Kinny, P. D., Sheraton, J. W. & Delor, C. P. (1991). Rapid production and evolution of late Archaean felsic crust in the Vestfold Block of East Antarctica. *Precambrian Research* **50**, 283–310.

Black, L. P., Kamo, S. L., Allen, C. M., Aleinikoff, J. N., Davis, D. W., Korsch, R. J. & Foudoulis, C. (2003). TEMORA 1: a new standard for Phanerozoic U–Pb geochronology. *Chemical Geology* **200**, 155–170.

Board, W. S., Frimmel, H. E. & Armstrong, R. A. (2005). Pan-African tectonism in the western Maud belt: P–T–t path for high-grade gneisses in the H. U. Sverdrupfjiella, East Antarctica. *Journal of Petrology* **46**, 671–699.

Boger, S. D. & White, R. W. (2003). The metamorphic evolution of metapelitic granulites from Radok Lake, northern Prince Charles Mountains, east Antarctica; evidence for an anticlockwise P–T path. *Journal of Metamorphic Geology* **21**, 285–298.

Boger, S. D. & Wilson, C. J. L. (2005). Early Cambrian crustal shortening and a clockwise P–T–t path from the southern Prince Charles Mountains, East Antarctica: implications for the formation of Gondwana. *Journal of Metamorphic Geology* **23**, 603–623.

Boger, S. D., Carson, C. J., Wilson, C. J. L. & Fanning, C. M. (2000). Neoproterozoic deformation in the northern Prince Charles Mountains, East Antarctica: evidence for a single protracted orogenic event. *Precambrian Research* **104**, 1–24.

Boger, S. D., Wilson, C. J. L. & Fanning, C. M. (2001). Early Paleozoic tectonism within the East Antarctic craton: the final suture between east and west Gondwana? *Geology* **29**, 463–466.

Boger, S. D., Carson, C. J., Fanning, C. M., Hergt, J. M., Wilson, C. J. L. & Woodhead, J. D. (2002). Pan-African intraplate deformation in the northern Prince Charles Mountains, East Antarctica. *Earth and Planetary Science Letters* **195**, 195–210.

Boger, S. D., Wilson, C. J. L. & Fanning, C. M. (2006). An Archaean province in the southern Prince Charles Mountains, East Antarctica: U–Pb zircon evidence for *c.* 3170 Ma granite plutonism and *c.* 2780 Ma partial melting and orogenesis. *Precambrian Research* **145**, 207–228.

Burton, K. W., Kohn, M. G., Cohen, A. S. & O'Nions, R. K. (1995). The relative diffusion of Pb, Nd, Sr and O in garnet. *Earth and Planetary Science Letters* **133**, 199–211.

Carson, C. J., Dirks, P. G. H. M., Hand, M., Sims, J. P. & Wilson, C. J. L. (1995). Compressional and extensional tectonics in low–medium pressure granulites from the Larsemann Hills, East Antarctica. *Geological Magazine* **132**, 151–170.

Carson, C. J., Fanning, C. M. & Wilson, C. J. L. (1996). Timing of the Progress Granite, Larsemann Hills: evidence for Early Palaeozoic orogenesis within the East Antarctica Shield and implications for Gondwana assembly. *Australian Journal of Earth Sciences* **43**, 539–553.

Carson, C. J., Powell, P., Wilson, C. J. L. & Dirks, P. H. G. M. (1997). Partial melting during tectonic exhumation of a granulite terrane: an example from the Larsemann Hills, East Antarctica. *Journal of Metamorphic Geology* **15**, 105–126.

Carson, C. J., Boger, S. D., Fanning, C. M., Wilson, C. J. L. & Thost, D. E. (2000). SHRIMP U–Pb geochronology from Mount Kirkby, northern Prince Charles Mountains, East Antarctica. *Antarctic Science* **12**, 429–442.

Chacko, T., Lamb, M. & Farquhar, J. (1996). Ultra-high temperature metamorphism in the Kerala Khondalite Belt. In: Santosh, M. & Yoshida, M. (eds) *The Archean and Proterozoic Terrains in Southern India within Gondwana. Gondwana Research Group Memoir* **3**, 157–165.

Cherniak, D. J. & Watson, E. B. (2001). Pb diffusion in zircon. *Chemical Geology* **172**, 5–24.

Cohen, A. S., O'Nions, R. K., Siegenthaler, R. & Griffin, W. L. (1988). Chronology of the pressure–temperature history recorded by a granulite terrain. *Contributions to Mineralogy and Petrology* **98**, 303–311.

Corvino, A. F., Boger, S. D., Wilson, C. J. L. & Fitzsimons, I. C. W. (2005). Geology and SHRIMP U–Pb zircon chronology of the Clemence Massif, central Prince Charles Mountains, East Antarctica. *Terra Antartica* **12**, 55–68.

Dale, J., Holland, T. & Powell, R. (2000). Hornblende–garnet–plagioclase thermobarometry: a natural assemblage calibration of the thermodynamics of hornblende. *Contributions to Mineralogy and Petrology* **140**, 353–362.

Dalziel, I. W. D. (1991). Pacific margins of Laurentia and East Antarctica–Australia as a conjugate rift pair: evidence and implications for an Eocambrian supercontinent. *Geology* **19**, 598–601.

Deer, W. A., Howie, R. A. & Zussman, J. (1992). edn. *An Introduction to Rock-forming Minerals*, 2nd edn. Harlow: Longman.

Dirks, P. H. G. M. & Hand, M. (1995). Clarifying P–T paths via structures in granulite from the Bolingen Islands, Antarctica. *Australian Journal of Earth Sciences* **42**, 157–172.

Dirks, P. H. G. M. & Wilson, C. J. L. (1995). Crustal evolution of the East Antarctic mobile belt in Prydz Bay: continental collision at 500 Ma? *Precambrian Research* **75**, 189–207.

Droop, G. T. R. (1987). A general equation for estimating Fe^{3+} concentrations in ferromagnesian silicates and oxides from microprobe analyses, using stoichiometric criteria. *Mineralogical Magazine* **51**, 431–435.

Fitzsimons, I. C. W. (1996). Metapelitic migmatites from Brattstrand Bluffs, East Antarctica—metamorphism, melting and exhumation of the mid crust. *Journal of Petrology* **37**, 395–414.

Fitzsimons, I. C. W. (2000). A review of tectonic events in the East Antarctic Shield and their implications for Gondwana and earlier supercontinents. *Journal of African Earth Sciences* **31**, 3–23.

Fitzsimons, I. C. W. (2003). Proterozoic basement provinces of southern and southwestern Australia, and their correlation with Antarctica. In: Yoshida, M., Windley, B. & Dasgupta, S. (eds) *Proterozoic East Gondwana: Supercontinent Assembly and Breakup. Geological Society, London, Special Publications* **206**, 93–130.

Fitzsimons, I. C. W. & Harley, S. L. (1991). Geological relationships in high-grade gneisses of the Brattstrand Bluffs coastline, Prydz Bay, East Antarctica. *Australian Journal of Earth Sciences* **38**, 497–519.

Fitzsimons, I. C. W. & Harley, S. L. (1992). Mineral reaction textures in high grade gneisses, evidence for contrasting pressure–temperature paths in the Proterozoic complex of east Antarctica. In: Yoshida, Y., Kaminuma, K. & Shiraishi, K. (eds) *Recent Progress in Antarctic Earth Science*. Tokyo: Terra, pp. 103–111.

Fitzsimons, I. C. W. & Harley, S. L. (1994*a*). Garnet coronas in scapolite–wollastonite calc-silicates from East Antarctica: the application and limitation of activity corrected grids. *Journal of Metamorphic Geology* **12**, 761–777.

Fitzsimons, I. C. W. & Harley, S. L. (1994*b*). The influence of retrograde cation exchange on granulite *P–T* estimates and a convergence technique for the recovery of peak metamorphic conditions. *Journal of Petrology* **35**, 543–576.

Fitzsimons, I. C. W., Kinny, P. D. & Harley, S. L. (1997). Two stages of zircon and monazite growth in anatectic leucogneiss: SHRIMP constraints on the duration and intensity of Pan-African metamorphism in Prydz Bay, East Antarctica. *Terra Nova* **9**, 47–51.

Green, D. H. & Ringwood, A. E. (1967). An experimental investigation of the gabbro to eclogite transformation and its petrological applications. *Geochimica et Cosmochimica Acta* **31**, 767–833.

Grew, E. S. & Manton, W. I. (1981). Geochronologic studies in East Antarctica: ages of rocks at Reinbolt Hills and Molodezhnaya Station. *Antarctic Journal of the United States* **16**, 5–7.

Hand, M., Scrimgeour, I., Powell, R., Stüwe, K. & Wilson, C. J. L. (1994). Metapelitic granulites from Jetty Peninsula, east Antarctica: formation during a single event or by polymetamorphism? *Journal of Metamorphic Geology* **12**, 557–573.

Harley, S. L. (1984). An experimental study of the partitioning of Fe and Mg between garnet and orthopyroxene. *Contributions to Mineralogy and Petrology* **86**, 359–373.

Harley, S. L. (1987). Precambrian geological relationships in high-grade gneisses of the Rauer Islands, east Antarctica. *Australian Journal of Earth Science* **34**, 175–207.

Harley, S. L. (1988). Proterozoic granulites from the Rauer Group, East Antarctica. I. Decompressional pressure–temperature paths deduced from mafic and felsic gneisses. *Journal of Petrology* **29**, 1059–1095.

Harley, S. L. (1989). The origins of granulites: a metamorphic perspective. *Geological Magazine* **126**, 215–247.

Harley, S. L. (1998). Ultrahigh temperature granulite metamorphism (1,050°C, 12 kbar) and decompression in garnet (Mg_{70})–orthopyroxene–sillimanite gneisses from the Rauer Group, East Antarctica. *Journal of Metamorphic Geology* **16**, 541–562.

Harley, S. L. (2003). Archaean–Cambrian crustal development of East Antarctica: metamorphic characteristics and tectonic implications. In: Yoshida, M., Windley, B. & Dasgupta, S. (eds) *Proterozoic East Gondwana: Supercontinent Assembly and Breakup. Geological Society, London, Special Publications* 206, 203–230.

Harley, S. L. & Fitzsimons, I. C. W. (1991). Pressure–temperature evolution of metapelitic granulites in a polymetamorphic terrane: the Rauer Group, East Antarctica. *Journal of Metamorphic Geology* **9**, 231–243.

Harley, S. L. & Green, D. H. (1982). Garnet–orthopyroxene barometry for granulites and peridotites. *Nature* **300**, 697–701.

Harley, S. L., Snape, I. & Black, L. P. (1998). The early evolution of a layered metaigneous complex in the Rauer Group, East Antarctica: evidence for a distinct Archaean terrane. *Precambrian Research* **89**, 175–205.

Harris, P. D., Moyes, A. B., Fanning, C. M. & Armstrong, R. A. (1995). Zircon ion microprobe results from the Maudheim high-grade gneiss terrane, western Dronning Maud Land, Antarctica. In: Barton, J. M. J. & Copperthwaite, Y. E. (eds) *Centennian Geocongress (1995)*. Johannesburg: Geological Society of South Africa, pp. 240–243.

Hensen, B. J. & Zhou, B. (1995). A Pan-African granulite facies metamorphic episode in Prydz Bay, Antarctica: evidence from Sm–Nd garnet dating. *Australian Journal of Earth Sciences* **42**, 249–258.

Hensen, B. J., Zhou, B. & Thost, D. E. (1995). Are reaction textures reliable guides to metamorphic histories? Timing constraints from garnet Sm–Nd chronology for 'decompression' textures in granulites from Søstrene Island, Prydz Bay, Antarctica. *Geological Journal* **30**, 261–271.

Hoffman, P. F. (1991). Did the breakout of Laurentia turn Gondwanaland inside out? *Science* **252**, 1409–1412.

Hokada, T., Harley, S. L. & Yokoyama, K. (2003). Peak and post-peak development of UHT metamorphism at Mather Peninsula, Rauer Islands: monazite U–Th–Pb and REE chemistry constraints. *Ninth International Symposium on Antarctic Earth Sciences, Abstracts, Potsdam, Germany*, pp. 161–162.

Holdaway, M. J., Mukhopadhyay, B., Dyar, M. D., Guidotti, C. V. & Dultrow, B. L. (1997). Garnet–biotite geothermometry revised: new Margules parameters and a natural specimen data set from Maine. *American Mineralogist* **82**, 582–595.

Holland, T. & Blundy, J. (1994). Non-deal interactions in calcic amphiboles and their bearing on amphibole–plagioclase thermometry. *Contributions to Mineralogy and Petrology* **116**, 433–447.

Holland, T. J. B. & Powell, R. (1998). An internally consistent thermodynamic dataset for phases of petrological interest. *Journal of Metamorphic Geology* **16**, 309–343.

Hoskin, P. W. O. & Black, L. P. (2000). Metamorphic zircon formation by solid-state recrystallization of protolith igneous zircon. *Journal of Metamorphic Geology* **18**, 423–439.

Humphries, F. J. & Cliff, R. A. (1982). Sm–Nd dating and cooling history of Scourian granulites, Sutherland, NW Scotland. *Nature* **295**, 515–517.

Ito, K. & Kennedy, C. (1971). An experimental study of the basalt–garnet granulite–eclogite transition. In: Heacock, J. G. (ed.) *The Structural and Physical Properties of the Earth's Crust. Geophysical Monograph, American Geophysical Union* **14**, 303–314.

Jacobs, J., Fanning, C. M., Henjes-Kunst, F., Olesch, M. & Paech, H.-J. (1998). Continuation of the Mozambique Belt into East Antarctica: Grenville-age metamorphism and polyphase Pan-African high-grade events in central Dronning Maud Land. *Journal of Geology* **106**, 385–406.

Jacobs, J., Bauer, W. & Fanning, C. M. (2003). Late Neoproterozoic/Early Palaeozoic events in central Dronning Maud Land and significance for the southern extension of the East African Orogen into East Antarctica. *Precambrian Research* **126**, 27–53.

Jagoutz, E. (1988). Nd and Sr systematics in an eclogite xenolith from Tanzania: evidence for frozen mineral equilibria in the continental lithosphere. *Geochimica et Cosmochimica Acta* **52**, 1285–1293.

Jahn, B.-M., Liu, X. C., Yui, T.-F., Morin, N. & Coz, M. B.-L. (2005). High-pressure/ultrahigh-pressure eclogites from the Hong'an Block, east–central China: geochemical characterization, isotope

disequilibrium and geochronological controversy. *Contributions to Mineralogy and Petrology* **149**, 499–526.

Jones, K. A. & Escher, J. C. (2002). Near-isothermal decompression within a clockwise *P–T* evolution recorded in migmatitic mafic granulites from Clavering Ø, NE Greenland: implications for the evolution of the Caledonides. *Journal of Metamorphic Geology* **20**, 365–378.

Kelly, N. M., Clarke, G. L. & Fanning, C. M. (2002). A two-stage evolution of the Neoproterozoic Rayner Structural Episode: new U–Pb sensitive high resolution ion microprobe constraints from the Oygarden Group, Kemp Land, East Antarctica. *Precambrian Research* **116**, 307–330.

Kelsey, D. E., Powell, R., Wilson, C. J. L. & Steele, D. A. (2003*a*). (Th + U)–Pb monazite ages from Al–Mg-rich metapelites, Rauer Group, East Antarctica. *Contributions to Mineralogy and Petrology* **146**, 326–340.

Kelsey, D. E., White, R. W., Powell, R., Wilson, C. J. L. & Quinn, C. D. (2003*b*). New constraints on metamorphism in the Rauer Group, Prydz Bay, east Antarctica. *Journal of Metamorphic Geology* **21**, 739–759.

Keto, L. S. & Jacobsen, S. B. (1987). Nd and Sr isotopic variations of Early Paleozoic oceans. *Earth and Planetary Science Letters* **84**, 27–41.

Kinny, P. D., Black, L. P. & Sheraton, J. W. (1993). Zircon ages and the distribution of Archean and Proterozoic rocks in the Rauer Islands. *Antarctic Science* **5**, 193–206.

Kinny, P. D., Black, L. P. & Sheraton, J. W. (1997). Zircon U–Pb ages and geochemistry of igneous and metamorphic rocks in the northern Prince Charles Mountains, Antarctica. *AGSO Journal of Australian Geology & Geophysics* **16**, 637–654.

Kretz, R. (1983). Symbols for rock-forming minerals. *American Mineralogist* **68**, 277–279.

Lee, J., Williams, I. & Ellis, D. (1997). Pb, U and Th diffusion in nature zircon. *Nature* **390**, 159–162.

Liermann, H.-P., Isachsen, C., Altenberger, U. & Oberhänsli, R. (2002). Behavior of zircon during high-pressure, low-temperature metamorphism: case study from the Internal Unit of the Sesia Zone (Western Italian Alps). *European Journal of Mineralogy* **14**, 61–71.

Liu, X. C., Zhao, Y. & Liu, X. H. (2002). Geological aspects of the Grove Mountains, East Antarctica. In: Gamble, J. A., Skinner, D. N. B. & Henrys, S. (eds) *Antarctica at the Close of a Millennium. Royal Society of New Zealand Bulletin* **35**, 161–166.

Liu, X. C., Zhao, Z., Zhao, Y., Chen, J. & Liu, X. H. (2003). Pyroxene exsolution in mafic granulites from the Grove Mountains, East Antarctica: constraints on the Pan-African metamorphic conditions. *European Journal of Mineralogy* **15**, 55–65.

Liu, X. C., Jahn, B.-M., Zhao, Y., Li, M., Li, H. & Liu, X. H. (2006). Late Pan-African granitoids from the Grove Mountains, East Antarctica: age, origin and tectonic implications. *Precambrian Research* **145**, 131–154.

Liu, X. C., Jahn, B.-M., Zhao, Y., Zhao, G. & Liu, X. H. (2007). Geochemistry and geochronology of high-grade rocks from the Grove Mountains, East Antarctica: evidence for an Early Neoproterozoic basement metamorphosed during a single Late Neoproterozoic/Cambrian tectonic cycle. *Precambrian Research* doi:10.1016/j.precamres.2007.04.005.

Ludwig, K. R. (1999). Isoplot/Ex (v. 2.06)—a geochronological toolkit for Microsoft Excel. *Berkeley Geochronology Center, Special Publication* **1a**, 49 pp.

Manton, W. I., Grew, E. S., Ghofmann, J. & Sheraton, J. W. (1992). Granitic rocks of the Jetty Peninsula, Amery Ice Shelf area, East Antarctica. In: Yoshida, Y., Kaminuma, K. & Shiraishi, K. (eds) *Recent Progress in Antarctic Earth Science*. Tokyo: Terra, pp. 179–189.

Mezger, K., Essene, E. J. & Halliday, A. N. (1992). Closure temperatures of the Sm–Nd system in metamorphic garnets. *Earth and Planetary Science Letters* **113**, 397–409.

Mikhalsky, E. V., Laiba, A. A., Beliatsky, B. V. & Stüwe, K. (1999). Geology, age and origin of the Mount Willing area (Prince Charles Mountains, East Antarctica). *Antarctic Science* **11**, 338–352.

Mikhalsky, E. V., Sheraton, J. W., Laiba, A. A., Tingey, R. J., Thost, D. E., Kamenev, E. N. & Fedorov, L. V. (2001). Geology of the Prince Charles Mountains, Antarctica. *AGSO-Geoscience Australia Bulletin* **247**, 1–209.

Mikhalsky, E. V., Laiba, A. A. & Beliatsky, B. V. (2006). Tectonic subdivision of the Prince Charles Mountains: a review of geologic and isotopic data. In: Fütterer, D. K., Damaske, D., Kleinschmidt, G., Miller, H. & Tessensohn, F. (eds) *Antarctica: Contributions to Global Earth Sciences*. Berlin Heidelberg New York: Springer-Verlag, pp. 69–82.

Möller, A., O'Brien, P. J., Kennedy, A. & Kröner, A. (2003). The use and abuse of Th–U ratios in the interpretation of zircon. *Geophysical Research Abstracts* **5**, 12113.

Moores, E. M. (1991). Southwest U. S.–East Antarctic (SWEAT) connection: a hypothesis. *Geology* **19**, 425–428.

Motoyoshi, Y., Thost, D. E. & Hensen, B. J. (1991). Reaction textures in calc-silicate granulites from the Bolingen Islands, Prydz Bay, East Antarctica: implications for the retrograde *P–T* path. *Journal of Metamorphic Geology* **9**, 293–300.

Nichols, G. T. & Berry, R. F. (1991). A decompressional *P–T* path, Reinbolt Hills, East Antarctica. *Journal of Metamorphic Geology* **9**, 257–266.

Pattison, D. R. M. & Bégin, N. J. (1994). Zoning patterns in orthopyroxene and garnet in granulites: implications for geothermometry. *Journal of Metamorphic Geology* **12**, 387–410.

Pattison, D. R. M., Chacko, T., Farquhar, J. & McFarlane, C. R. M. (2003). Temperatures of granulite-facies metamorphism: constraints from experimental phase equilibria and thermobarometry corrected for retrograde exchange. *Journal of Petrology* **44**, 867–900.

Paulsson, O. & Austrheim, H. (2003). A geochronological and geochemical study of rocks from Gjesvikfjella, Dronning Maud Land, Antarctica—implications for Mesoproterozoic correlations and assembly of Gondwana. *Precambrian Research* **125**, 113–138.

Phillips, G., Wilson, C. J. L., Campbell, I. H. & Allen, C. M. (2006). U–Th–Pb detrital zircon geochronology from the southern Prince Charles Mountains, East Antarctica—defining the Archaean to Neoproterozoic Ruker Province. *Precambrian Research* **148**, 292–306.

Post, N. J., Hensen, B. J. & Kinny, P. D. (1997). Two metamorphic episodes during a 1340–1180 Ma convergent tectonic event in the Windmill Islands, East Antarctica. In: Ricci, C. A. (ed.) *The Antarctic Region: Geological Evolution and Processes*. Siena: Terra Antartica, pp. 157–161.

Powell, R. & Holland, T. (1988). An internally consistent dataset with uncertainties and correlations: 3. Applications to geobarometry, worked examples and a computer program. *Journal of Metamorphic Geology* **6**, 173–204.

Powell, R. & Holland, T. (1994). Optimal geothermometry and geobarometry. *American Mineralogist* **79**, 120–133.

Ren, L., Zhao, Y., Liu, X. H. & Chen, T. (1992). Re-examination of the metamorphic evolution of the Larsemann Hills, East Antarctica. In: Yoshida, Y., Kaminuma, K. & Shiraishi, K. (eds) *Recent Progress in Antarctic Earth Science*. Tokyo: Terra, pp. 145–153.

Rubatto, D. & Gebauer, D. (2000). Use of cathodoluminescence for U–Pb zircon dating by ion microprobe; some example from the Western Alps. In: Pagel, M., Barbin, V., Blanc, P. &

Ohnenstetter, D. (eds) *Cathodoluminescence in Geosciences*. Berlin: Springer, pp. 373–400.

Rubatto, D., Gebauer, D. & Compagnoni, R. (1999). Dating of eclogite-facies zircons: the age of Alpine metamorphism in the Sesia–Lanzo Zone (Western Alps). *Earth and Planetary Science Letters* **167**, 141–158.

Rushmer, T. (1991). Partial melting of two amphibolites: contrasting experimental results under fluid-absent and fluid-present conditions. *Contributions to Mineralogy and Petrology* **107**, 41–59.

Salje, E. (1986). Heat capacities and entropies of andalusite and sillimanite. The influence of fibrolitisation on the phase diagram of the Al_2SiO_5 polymorphs. *American Mineralogist* **71**, 1366–1371.

Shackleton, R. M. (1996). The final collision zone between East and West Gondwana: where is it?. *Journal of African Earth Sciences* **23**, 271–287.

Sheraton, J. W., Black, L. P., McCulloch, M. T. & Oliver, R. L. (1990). Age and origin of a compositionally varied mafic dyke swarm in the Bunger Hills, East Antarctica. *Chemical Geology* **85**, 215–246.

Sheraton, J. W., Black, L. P. & Tindle, A. G. (1992). Petrogenesis of plutonic rocks in a Proterozoic granulite-facies terrane—the Bunger Hills, East Antarctica. *Chemical Geology* **97**, 163–198.

Sheraton, J. W., Tindle, A. G. & Tingey, R. J. (1996). Geochemistry, origin, and tectonic setting of granitic rocks of the Prince Charles Mountains, Antarctica. *AGSO Journal of Australian Geology & Geophysics* **16**, 345–370.

Shiraishi, K., Ellis, D. J., Hiroi, Y., Fanning, C. M., Motoyoshi, Y. & Nakai, Y. (1994). Cambrian orogenic belt in East Antarctica and Sri Lanka: implications for Gondwana assembly. *Journal Geology* **102**, 47–65.

Sims, J. P., Dirks, P. H. G. M., Carson, C. J. & Wilson, C. J. L. (1994). The structural evolution of the Rauer Group, East Antarctica: mafic dykes as passive markers in a composite Proterozoic terrain. *Antarctic Science* **6**, 379–394.

Snape, I. S., Black, L. P. & Harley, S. L. (1997). Refinement of the timing of magmatism and high-grade deformation in the Vestfold Hills, East Antarctica, from new SHRIMP U–Pb zircon geochronology. In: Ricci, C. A. (ed.) *The Antarctic Region: Geological Evolution and Processes*. Siena: Terra Antartica, pp. 139–148.

Spear, F. S., Kohn, M. J. & Cheney, J. T. (1999). *P–T* paths from anatectic pelites. *Contributions to Mineralogy and Petrology* **34**, 7–32.

Stacey, J. S. & Kramers, J. D. (1975). Approximation of terrestrial lead isotope evolution by two-stage model. *Earth and Planetary Science Letters* **26**, 207–221.

Stephenson, N. C. N. & Cook, N. D. J. (1997). Metamorphic evolution of calc-silicate granulites near Battye Glacier, northern Prince Charles Mountains, east Antarctica. *Journal of Metamorphic Geology* **15**, 361–378.

Thost, D. E., Hensen, B. J. & Motoyoshi, Y. (1991). Two-stage decompression in garnet-bearing mafic granulites from Søstrene Island, Prydz Bay, East Antarctica. *Journal of Metamorphic Geology* **9**, 245–256.

Thost, D. E., Hensen, B. J. & Motoyoshi, Y. (1994). The geology of a rapidly uplifted medium and low pressure granulite facies terrane of Pan African age: the Bolingen Islands, Prydz Bay, East Antarctica. *Petrology* **2**, 293–316.

Tingey, R. J. (1981). Geological investigations in Antarctica 1968–1969: the Prydz Bay–Amery Ice Shelf–Prince Charles Mountains area. *Bureau of Mineral Resources, Australia, Record*, **1981/34.**

Tingey, R. J. (1991). The regional geology of Archaean and Proterozoic rocks in Antarctica. In: Tingey, R. J. (ed.) *The Geology of Antarctica*. Oxford: Oxford University Press, pp. 1–73.

Tong, L. & Liu, X. H. (1997). The prograde metamorphism of the Larsemann Hills, East Antarctica: evidence for an anticlockwise *P–T* path. In: Ricci, C. A. (ed.) *The Antarctic Region: Geological Evolution and Processes*. Siena: Terra Antartica, pp. 105–114.

Tong, L. & Wilson, C. J. L. (2006). Tectonothermal evolution of the ultrahigh temperature metapelites in the Rauer Group, east Antarctica. *Precambrian Research* **149**, 1–20.

Vavra, G., Gebauer, D., Schmid, R. & Compston, W. (1996). Multiple zircon growth and recrystallisation during polyphase Late Carboniferous to Triassic metamorphism in granulites of Ivrea Zone (Southern Alps): an ion microprobe (SHRIMP) study. *Contributions to Mineralogy and Petrology* **122**, 337–358.

Wang, Y., Liu, D., Ren, L. & Tang, S. (2003). Advances in SHRIMP geochronology and their constraints on understanding the tectonic evolution of Larsemann Hills, East Antarctica. *Ninth International Symposium on Antarctic Earth Sciences, Abstracts, Potsdam, Germany*, pp. 334–335.

White, R. W., Powell, R. & Holland, T. J. B. (2001). Calculation of partial melting equilibria in the system Na2O-CaO-K2O-FeoO-MgO-Al2O3-SiO2-H2O (NCKFMASH). *Journal of Metamorphic Geology* **19**, 139–153.

Williams, I. S. (1998). U–Th–Pb geochronology by ion microprobe. In: McKibben, M. A., Shanks, W. C. & Ridley, W. I. (eds) *Applications of Microanalytical Techniques to Understanding Mineralizing Processes. Reviews of Economic Geology* **7**, 1–35.

Williams, I. S. & Claesson, S. (1987). Isotopic evidence for the Precambrian provenance and Caledonian metamorphism of high grade paragneisses from the Seve Nappes, Scandinavian Caledonides: II. Ion microprobe zircon U–Th–Pb. *Contributions to Mineralogy and Petrology* **97**, 205–217.

Wilson, T. J., Grunow, A. M. & Hanson, R. E. (1997). Gondwana assembly: the view from southern Africa and East Gondwana. *Journal of Geodynamics* **23**, 263–286.

Yang, J.-H., Chung, S.-L., Zhai, M.-G. & Zhou, X.-H. (2004). Geochemical and Sr–Nd–Pb isotopic compositions of mafic dikes from the Jiaodong Peninsula, China: evidence for vein-plus-peridotite melting in the lithospheric mantle. *Lithos* **73**, 145–160.

Yoshida, M. (1995). Cambrian orogenic belt in East Antarctica and Sri Lanka: implications for Gondwana assembly: a discussion. *Journal of Geology* **103**, 467–468.

Yoshida, M., Jacobs, J., Santosh, M. & Rajesh, H. M. (2003). Role of Pan-African events in the Circum-East Antarctic Orogen of East Gondwana: a critical overview. In: Yoshida, M., Windley, B. & Dasgupta, S. (eds) *Proterozoic East Gondwana: Supercontinent Assembly and Breakup. Geological Society, London, Special Publications* **206**, 57–75.

Young, D. N. & Black, L. P. (1991). U–Pb zircon dating of Proterozoic igneous charnockites from the Mawson coast, east Antarctica. *Antarctic Science* **3**, 205–216.

Young, D. N., Zhao, J.-x., Ellis, D. J. & McCulloch, M. T. (1997). Geochemical and Sr–Nd isotopic mapping of source provinces for the Mawson charnockites, East Antarctica: implications for Proterozoic tectonics and Gondwana reconstruction. *Precambrian Research* **86**, 1–19.

Zhang, L., Tong, L., Liu, X. H. & Scharer, U. (1996). Conventional U–Pb age of the high-grade metamorphic rocks in the Larsemann Hills, East Antarctica. In: Pang, Z., Zhang, J. &

Sun, J. (eds) *Advances in Solid Earth Sciences*. Beijing: Science Press, pp. 27–35.

Zhao, J.-x., Ellis, D. E., Kilpatrick, J. A. & McCulloch, M. T. (1997*a*). Geochemical and Sr–Nd isotopic study of charnockites and related rocks in the northern Prince Charles Mountains, East Antarctica: implications for charnockite petrogenesis and Proterozoic crustal evolution. *Precambrian Research* **81**, 37–66.

Zhao, Y., Song, B., Wang, Y., Ren, L., Li, J. & Chen, T. (1992). Geochronology of the late granite in the Larsemann Hills, East Antarctica. In: Yoshida, Y., Kaminuma, K. & Shiraishi, K. (eds) *Recent Progress in Antarctic Earth Science*. Tokyo: Terra, pp. 155–161.

Zhao, Y., Liu, X. H., Song, B., Zhang, Z., Li, J., Yao, Y. & Wang, Y. (1995). Constraints on the stratigraphic age of metasedimentary rocks from the Larsemann Hills, East Antarctica: possible implications for Neoproterozoic tectonics. *Precambrian Research* **75**, 175–188.

Zhao, Y., Liu, X. H., Wang, S. & Song, B. (1997*b*). Syn- and post-tectonic cooling and exhumation in the Larsemann Hills, East Antarctica. *Episodes* **21**, 122–127.

Zhao, Y., Liu, X. C., Fanning, C. M. & Liu, X. H. (2000). The Grove Mountains, a segment of a Pan-African orogenic belt in East Antarctica. *Abstracts Volume of the 31th IGC, Rio de Janeiro, Brazil*.

Zhao, Y., Liu, X. H., Liu, X. C. & Song, B. (2003). Pan-African events in Prydz Bay, East Antarctica and its inference on East Gondwana tectonics. In: Yoshida, M., Windley, B. & Dasgupta, S. (eds) *Proterozoic East Gondwana: Supercontinent Assembly and Breakup. Geological Society, London, Special Publications* **206**, 231–245.

Ziemann, M. A., Förster, H.-J., Harlov, D. E. & Frei, D. (2005). Origin of fluorapatite–monazite assemblages in a metamorphosed, sillimanite-bearing pegmatoid, Reinbolt Hills, East Antarctica. *European Journal of Mineralogy* **17**, 567–579.